

Title: Optimization of supported cobalt catalysts for the Fischer-Tropsch Synthesis

Student: Mohamed Amine Lwazzani

Date: June 2023

Supervisor/s: Dr. Jordi Guilera Sala

Departament of Enginyeria Quimica

Dr. Andrés Alberto García Blanco

IREC

The Fischer-Tropsch synthesis is a process in which synthetic fuel can be produced from syngas. The interest of this fuel lies in its ability to foment a transition in hard to abate sectors such as aviation, heavy duty, and shipping.

The main objective of this investigation is to foment and research about the sustainability of synthetic fuels, by optimizing the catalysts and by upcycling CO₂ into fuels. These objectives were studied in 2 phases: The first phase focalized in the optimization of supported cobalt catalysts by varying their preparation technique and the cobalt loading, whilst for the second stage, cerium oxide is added to the optimized catalyst as promoter, for studying the effect of the cerium oxide on the conversion of CO/CO₂/H₂ mixtures.

The obtained catalysts were characterized by TPR, N₂ Adsorption, SEM, EDX, XRD, ICP-AES and CO chemisorption; and tested for Fischer Tropsch synthesis in a fixed-bed reactor at 2.0 MPa, 230 °C and a H₂/CO ratio of 2.

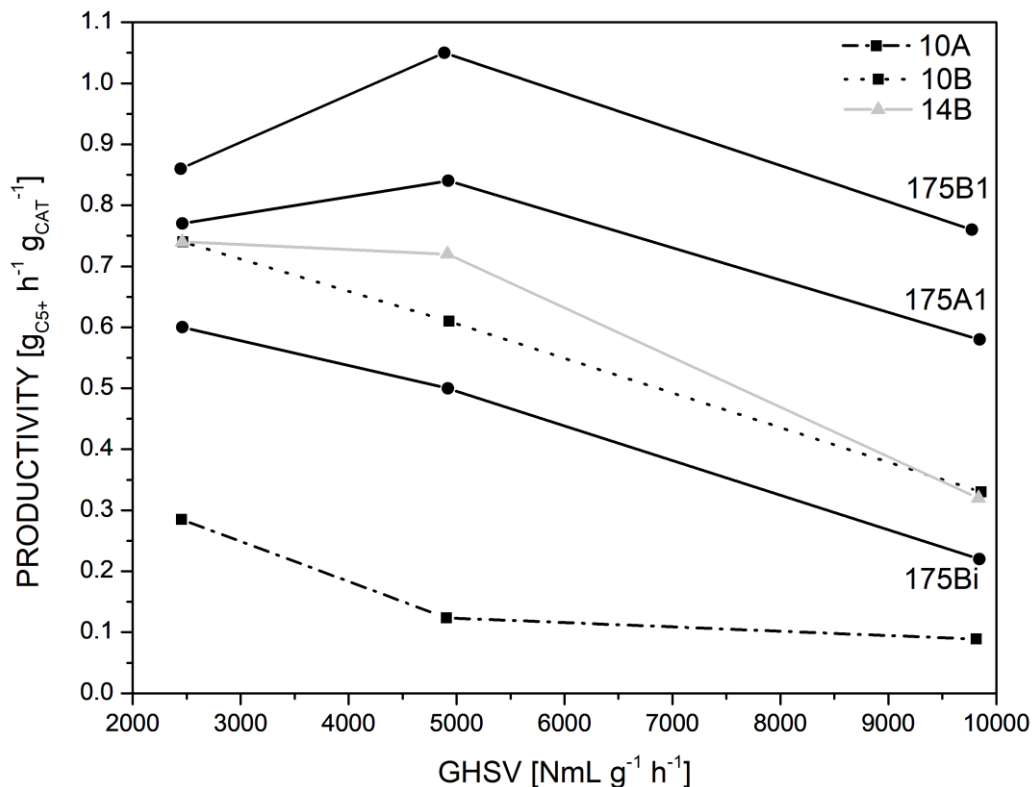


Figure 1: Productivity of the Supported Cobalt catalysts.

Differences between the supported cobalt catalysts were observed and related to the preparation method. The impregnation of Co^{2+} and Ce^{3+} resulted in a uniform distribution on the catalyst pellets. Lower calcination temperatures and unique impregnation led to higher reducibility of the cobalt oxides, and enhanced properties (S_{BET} , Metallic Surface Area, Dispersion, Particle Size) in comparison to the higher calcination temperature. The properties of the catalysts affected the catalytic performance of the catalysts, as seen in the Figure 1.

Once selected the optimized catalyst, a new batch of catalysts impregnated with cerium are prepared in the same conditions. These catalysts were tested under 2 syngas mixtures, in which one syngas mixture was enriched with 25 vol% of CO_2 , and the other one had no CO_2 in it.

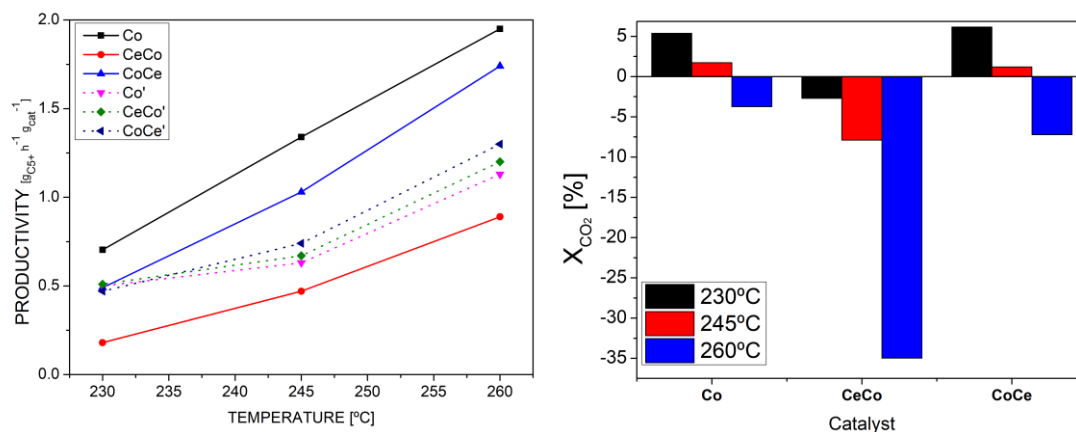


Figure 2: Left: Productivity of the Ceria-promoted catalysts. Right: Conversion of CO_2 for the Ce-promoted catalysts.

The reaction under a CO_2 -enriched mixture yields a lower productivity in comparison to the syngas (Figure 2: Left), these results are plausible because the CO_2 is not as reactive as the CO . Nonetheless, CO_2 conversion is detected at lower temperatures whilst for the highest temperature CO_2 is produced (Figure 2: Right). Cerium oxide improved the productivity obtained for the CO_2 -containing mixture in comparison to the non-promoted catalyst. Impregnation of the cobalt over the cerium oxide yields in higher CO_2 concentrations than cerium oxide impregnated over cobalt.



Màster en Enginyeria Química

Tutor/s

Dr. Jordi Guilera Sala
Departament Enginyeria Química
Dr. Andrés Alberto García Blanco
IREC

Treball Final de Màster

**Optimization of supported cobalt catalysts for the Fischer-Tropsch
Synthesis**

**Optimización de catalizadores de soportados de cobalto para la síntesis
de Fischer-Tropsch**

Mohamed Amine Lwazzani

June, 2023



UNIVERSITAT DE
BARCELONA

Dos campus d'excel·lència internacional

B:KC Barcelona
Knowledge
Campus

HUB^c Health Universitat
de Barcelona
Campus

Aquesta obra esta subjecta a la llicència de
Reconeixement-NoComercial-SenseObraDerivada



<http://creativecommons.org/licenses/by-nc-nd/3.0/es/>

REPORT

Contents

1. Summary:	9
2. Introduction:	11
2.2. The Fischer Tropsch Synthesis:	13
2.3. Fischer-Tropsch Synthesis Catalysts:	14
2.4. Reaction:	16
3. Objectives:	18
4. Methodology:	19
4.1. Impregnation:	19
4.2. Material Characterization:	20
4.3. Reaction	22
4.3.1. Setup:	22
4.3.2. Procedure:	23
4.3.3. Catalytic Test:	23
4.3.4. Calculations:	25
5. Results:	27
5.1. Characterization:	27
5.1.1. Density and ICP%:	27
5.1.2. SEM	29
5.1.3. N ₂ Adsorption:	30
5.1.4. XRD	32
5.1.5. TPR	35
5.1.6. CO Chemisorption:	37
5.1.7. Main Findings	39
5.2. Reaction:	40
5.2.1. Optimization of the Cobalt catalysts:	40
5.2.2. Ceria-promoted catalysts:	45
6. Conclusions:	53
7. Outlook:	54
8. Bibliography	55

1. Summary:

The Fischer-Tropsch synthesis is a process in which synthetic fuel can be produced from syngas. The interest of this fuel lies in its ability to foment a transition in hard to abate sectors such as aviation, heavy duty, and shipping.

The main objective of this investigation is to foment and research about the sustainability of synthetic fuels, by optimizing the catalysts and by upcycling CO₂ into fuels. These objectives were studied in 2 phases: The first phase focalized in the optimization of supported cobalt catalysts by varying their preparation technique and the cobalt loading, whilst for the second stage, cerium oxide is added to the optimized catalyst as promoter, for studying the effect of the cerium oxide on the conversion of CO/CO₂/H₂ mixtures.

The obtained catalysts were characterized by TPR, N₂ Adsorption, SEM, EDX, XRD, ICP-AES and CO chemisorption; and tested for Fischer Tropsch synthesis in a fixed-bed reactor at 2.0 MPa, 230 °C and a H₂/CO ratio of 2.

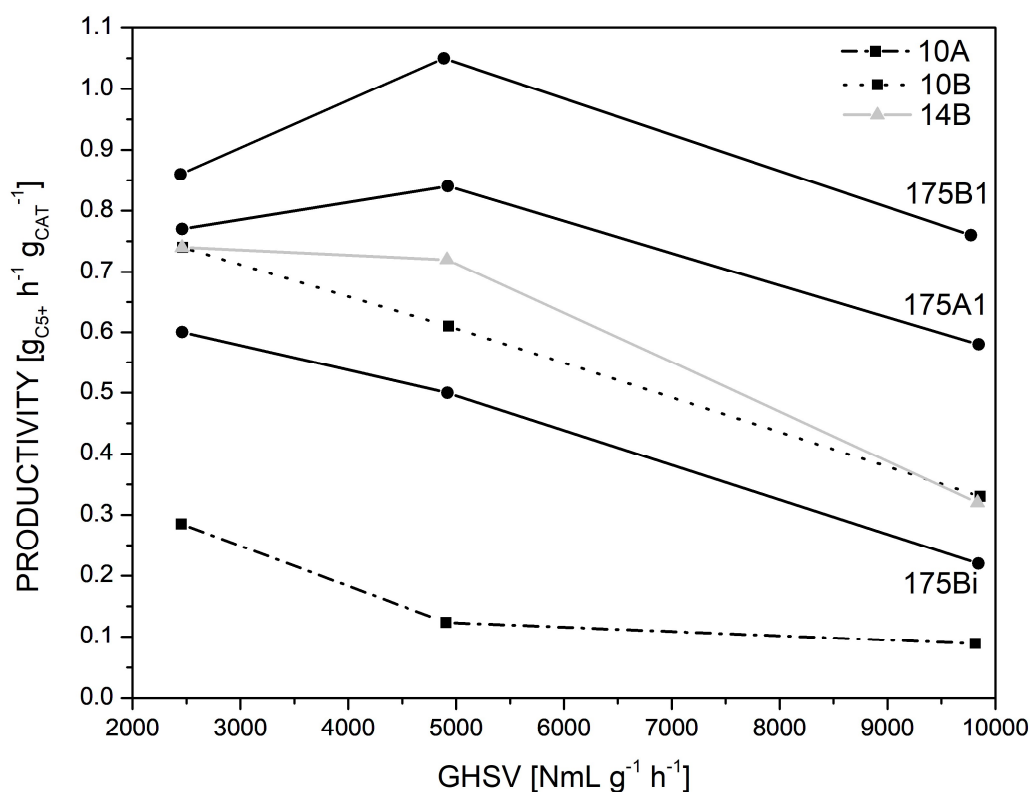


Figure 1: Productivity of the Supported Cobalt catalysts.

Differences between the supported cobalt catalysts were observed and related to the preparation method. The impregnation of Co^{2+} and Ce^{3+} resulted in a uniform distribution on the catalyst pellets. Lower calcination temperatures and unique impregnation led to higher reducibility of the cobalt oxides, and enhanced properties (S_{BET} , Metallic Surface Area, Dispersion, Particle Size) in comparison to the higher calcination temperature. The properties of the catalysts affected the catalytic performance of the catalysts, as seen in the Figure 1.

Once selected the optimized catalyst, a new batch of catalysts impregnated with cerium are prepared in the same conditions. These catalysts were tested under 2 syngas mixtures, in which one syngas mixture was enriched with 25 vol% of CO_2 , and the other one had no CO_2 in it.

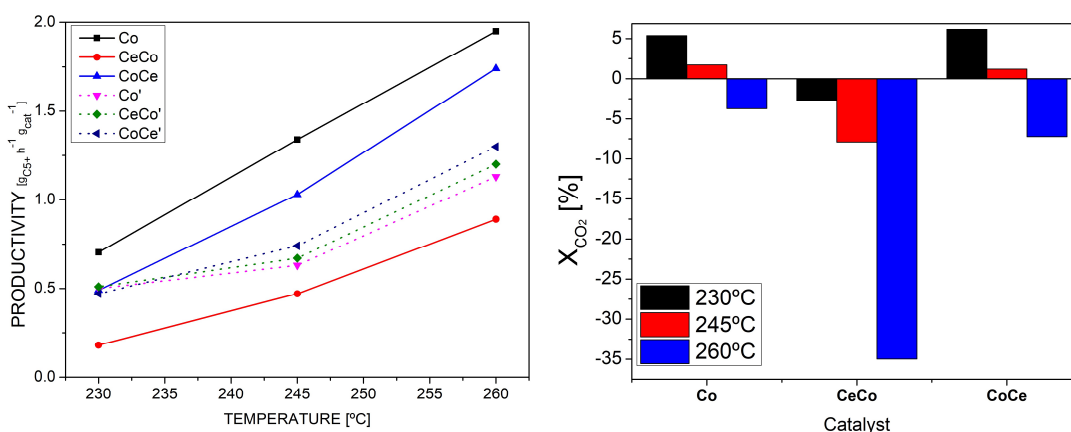


Figure 2: Left: Productivity of the Ceria-promoted catalysts. Right: Conversion of CO_2 for the Ce-promoted catalysts.

The reaction under a CO_2 -enriched mixture yields a lower productivity in comparison to the syngas (Figure 2: Left), these results are plausible because the CO_2 is not as reactive as the CO . Nonetheless, CO_2 conversion is detected at lower temperatures whilst for the highest temperature CO_2 is produced (Figure 2: Right). Cerium oxide improved the productivity obtained for the CO_2 -containing mixture in comparison to the non-promoted catalyst. Impregnation of the cobalt over the cerium oxide yields in higher CO_2 concentrations than cerium oxide impregnated over cobalt.

2. Introduction:

It is no news that CO₂ emissions are rising, climate change is a tangible threat, petroleum is ending, and we are still left with an endless bunch of reasons threatening our way of life. The aim of this work is to contribute to the study of an alternative for making front to some of these problems and threats (partially) by studying and analyzing the optimization of supported cobalt catalysts for the Fischer-Tropsch synthesis (FTS). The FTS is a set of chemical reactions that happen simultaneously (in parallel and in series) in which synthetic fuel is obtained, this synthetic fuel is obtained by reacting hydrogen and carbon monoxide, and ideally CO₂. If the used hydrogen/monoxide mixture, syngas from now on, comes from renewable resources, such as biomass or by CO₂ co-electrolysis, then the synthetic fuel is also renewable (Martinelli, et al. 2020), or at least partially (depending on the process) (Jones, Krexner and Bismarck 2022) (Shehesh and Dasappa 2016).

The importance of the FTS doesn't lie exclusively on the valorization of residual biomass or the transformation of renewable energy surplus in synfuel but in its strategical use to achieve the energy transition. Many efforts are made to achieve a transition to a sustainable model by electrification, nonetheless, electrification has its limits and can't reach all sectors (VAN NUFFEL, et al. 2018).

As Van Nuffel discusses in his report for the European Parliament, the energy transition must pass through sector coupling, "as a strategy to provide greater flexibility to the energy system so that decarbonization can be achieved in a more cost-effective way". A coupling between different energy systems leads to a higher resilience of the overall network, thus making it necessary.

For instance, strategical sectors, such as aviation, shipping, heavy-duty, high-temperature ovens, Chemical manufacture, etc. are hardly electrifiable, and cannot transition to a sustainable model if alternatives, as the synfuel, are not taken in account (Jones, Krexner and Bismarck 2022). The main objective of the transition is to provide a reliable, accessible, affordable, and safe energy system that can meet our human needs. Lots of efforts are being directed towards "clean energy" by promoting the use of wind and solar based renewable energy, ignoring the importance of other energy vectors that can contribute to a sustainable energy system.

Sustainability can be reached by different pathways, and under current circumstances of crisis, it is vital to study and analyze the role of the alternatives without losing the objectives. Citing Van Nuffel: "The transition from a linear to a circular economy will also require increased substitution of abiotic materials with bio-based ones, which will increase demand for non-food biomass [...]". Jones et al (Jones, Krexner and Bismarck 2022) claim that the use of the liquid fuels, such as electrofuels (e-fuels) or biomass-derived fuels are necessary to achieve climate change goals within an acceptable timeframe.

2.1. Sustainable Development Goals

Sustainable development goals (UN 2015) are goals specified by the UN for achieving a better world. This project subscribes to the sustainable development goals by developing and studying the FTS, a process in which energy is transformed and stored in liquid fuels, in a process called as XtL (Energy-to-Liquid process). The developed SDG are described below in Table 1.

The main purpose of this project is to contribute with a sand grain in the best effort of innovation and research to help tackle down or at least to create a viable solution for mitigating the devastating effects of climate change.

Table 1: Sustainable Development Goals

	<p>7. AFFORDABLE AND CLEAN ENERGY: Optimizing the FTS and obtaining affordable and sustainable synthetic fuels are the main reasons why this goal is chosen. By creating liquid synfuels, the energy infrastructure can be reused in the green transition. Also, these synfuels are estimated to be produced from renewable energy surplus or from biomass upcycling, favoring clean processes.</p>
	<p>8. DECENT WORK AND ECONOMIC GROWTH: The synfuels enhance the economy by securing strategical sectors and helping them to transition to sustainable forms. By ensuring the use of synfuels, many sectors can keep with their normal activity and even grow in a sustainable way.</p>
	<p>9. INDUSTRY, INNOVATION, AND INFRASTRUCTURE: The implementation of FTS can help to assure and develop sustainable, resilient, and quality infrastructure. The FTS not only produces hydrocarbons for synthetic fuel, they also can provide chemical precursors for other industries for other synthesis processes.</p>

2.2. The Fischer Tropsch Synthesis:

The FTS is a chemical synthesis reaction in which hydrogen and carbon monoxide react to form hydrocarbons. The objective for using this synthesis reaction is to obtain long-chain hydrocarbons, in the $[C_{12}-C_{20}]$ range, because these chains can be used as substitutes of the current fuels. The sustainable part of this reaction arises when the syngas, the hydrogen/monoxide mixture, comes from sustainable sources (Martinelli, et al. 2020), or when CO_2 is used for the obtention of the synthetic fuel. In Figure 1, a brief scheme of the desired process is illustrated. The green rectangle represents this work's focus.

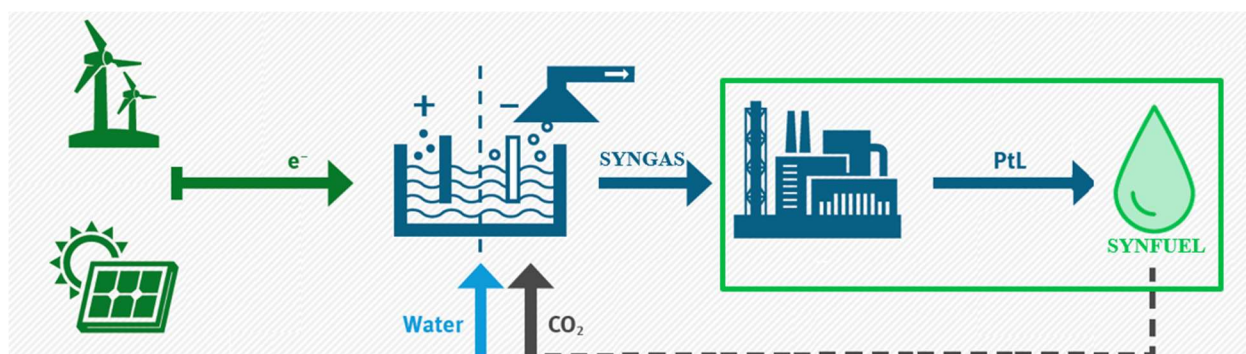


Figure 1: Synfuel production scheme

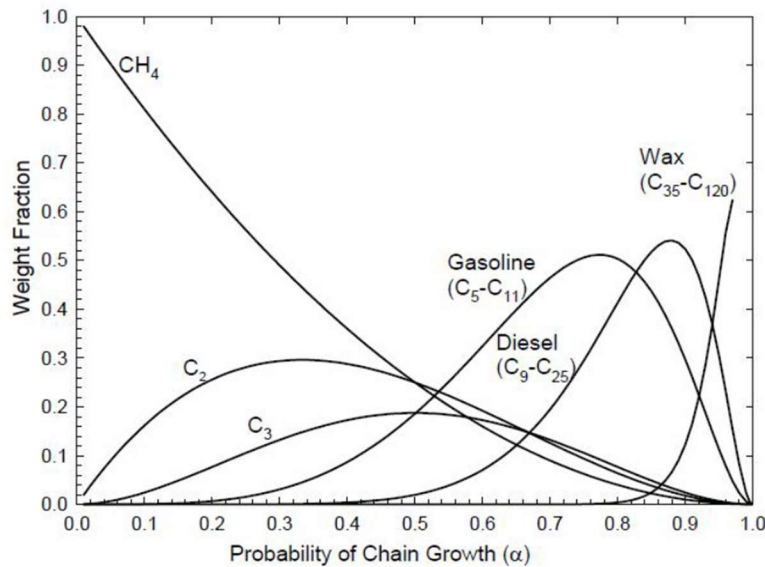
Figure 1 represents part of the overall process for the FTS incorporating renewable electricity and CO_2 recycling. Renewable energy surplus is used in a co-electrolysis cell for obtaining syngas, which is done as a form of energy-storage. For instance, countries like Spain, in punctual moments produce more energy than consumed. The energy surplus can be stored in batteries or in chemicals such as H_2 . Even if batteries or H_2 have a great potential offering solutions to the climate change, other alternatives, such as the FTS, cannot be minored.

The synfuels obtained by the FTS are energy-dense and can be used without major problems in existent infrastructure, synfuels do not imply a big change in current use of liquid fuels whilst batteries and H_2 do indeed need big inversions for the adaption of current infrastructure. Even if inversion is not problematic, hard to abate sectors, as described before, are hardly able to transition if not with the help of synfuels.

In the process shown in figure 1, the energy surplus is used to produce syngas, by CO_2 co-electrolysis. This syngas is then used for the obtention of the synfuel. This work focuses on this part, by optimizing the catalysts for the obtention of synfuels by means of FTS. The illustrated FTS process in Figure 1 is known inside the PtL, Power-to-Liquid, (techniques in which “Power”, Renewable electricity, is used and transformed into liquid fuels). The FTS is also involved in other techniques like BtL(Biomass), GtL(Gas-to-Liquid), CtL(Coal-to-liquid) XtL(General-process),. where different feedstocks are studied and analyzed for obtaining liquid fuels. The main route for the XtL processes passes by obtaining syngas, and then transforming this syngas into liquid fuels.

2.3. Fischer-Tropsch Synthesis Catalysts:

The FTS is a polymerization reaction that requires a catalyst to be carried out, see Figure 2, in which the product fractions are plotted against the probability of chain growth. Traditionally, the used catalysts are iron and cobalt, even if other metals can be used for the FTS (Mirzaei, et al. 2014), as shown in Figure 3.



The other metals (Ru, Rh...) are not used due to their economical accessibility and/or viability (Mirzaei, et al. 2014). Although cobalt prices are estimated at 6-10 times the iron's ones, they are best suited for long-chain hydrocarbon production (Martinelli, et al. 2020) while iron catalysts are better suited to produce intermediate products that can be used in other industries.

Figure 2: Anderson-Schulz-Flory distribution (Mirzaei, et al. 2014)

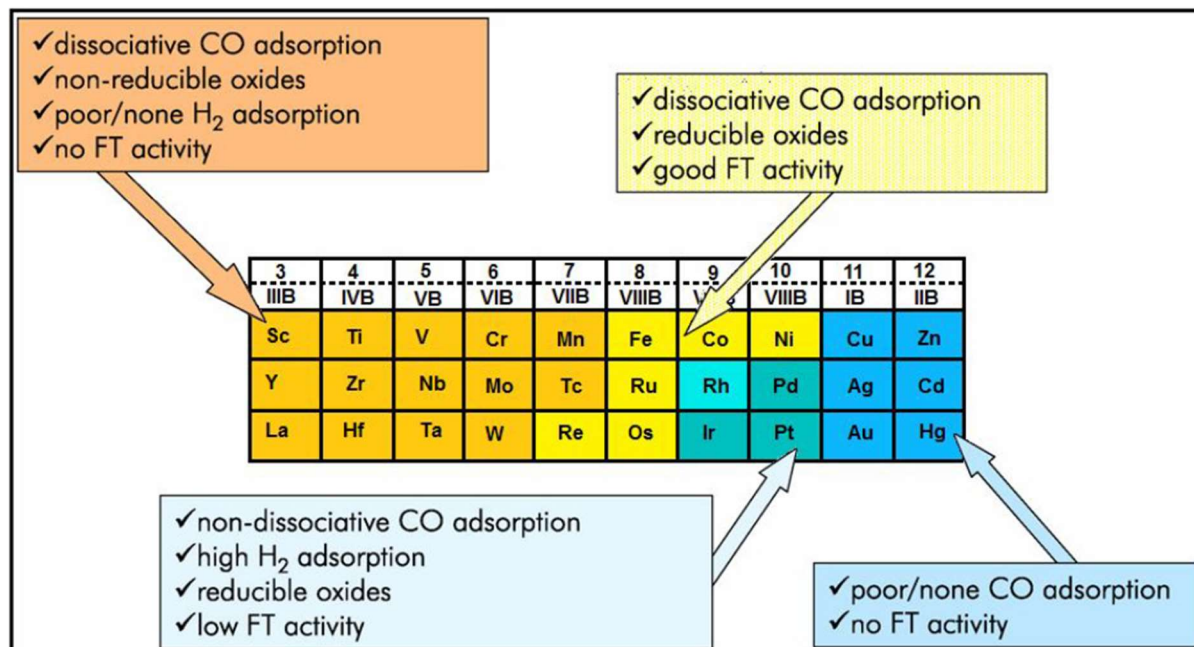


Figure 3: Transition metals behavior for FTS (Mirzaei, et al. 2014)

Cobalt based catalysts are chosen because of their selectivity to higher chain hydrocarbons. Once these catalysts are selected, they were synthesized by supporting a metal promoter on porous, thermally stable

and non-reactive material. The material must guarantee a high active surface and stability for carrying the reaction. (Małecka, et al. 2015). According to the literature, the catalytic performance depends on the catalyst preparation (Kraum and Baerns 1999) (Mirzaei, et al. 2014), and the catalyst properties, which can be affected by the following factors:

- Method of preparation
- Chemical nature of the Support
- Promoter
- Treatment

For (Małecka, et al. 2015), (Iglesia 1997) the properties that can be affected by the preparation are the particle Size, porosity, activity.

For the preparation of the catalyst, three main techniques are used: Co-Precipitation, in which the solid catalyst is precipitated from the solution and then recollected; Impregnation, in which a solid support is wetted by a promoter for obtaining the catalyst; and Sol-gel, in which the catalyst is produced by creating a gel-structure in which the metal is contained.

The impregnation method has been chosen because of its advantages giving high dispersion of the metal (Bezemer, et al. 2006) (Małecka, et al. 2015) and for being technologically not demanding, as the sol-gel technique, i.e. the impregnation method eliminates the large volumes of salt-containing solutions and the process separation of the Co-precipitation method (Mirzaei, et al. 2014).

In the literature, the use of various supports, such as silica, alumina, etc., are reported. However, γ -Al₂O₃ has been elected as support due to the characteristics it offers such as: Thermal stability, large surface area, little involvement in the FTS...

A precursor is used to disperse the cobalt on the support. In the literature (Mirzaei, et al. 2014) the use of acetate, sulfates, chlorides, nitrate, etc. is listed. The selection of the best precursor is done based on its effect on the cobalt distribution over the support. For example, nitrates are depicted by (Małecka, et al. 2015) (Zhang, et al. 2011) as the best precursors due their ease of decomposition into oxides, and also because they:

- The nitrates are dissolved with ease.
- They don't create a solid residue after decomposition like sulfates or chlorides, giving integrally oxides.
- Give materials of well-defined chemical composition.
- Lead to high specific surface area.

Once the support and the precursor have been selected and the impregnation is performed, the catalyst is calcined to decompose the nitrates into its oxides. This decomposition, depending on the conditions under which it is carried out, can lead to the loss of active metal, since cobalt tends to react with the alumina support at high temperatures, forming cobalt aluminate, which is an inactive species during FTS. This loss of active metal is also observed when other supports are used (Mirzaei, et al. 2014).

The calcined catalyst can be tested for FTS or can be promoted by cerium oxide with another impregnation. For the cerium-impregnation, Cerium nitrate is used, applying the same conditions as before for the cobalt salt. The reason why using cerium oxide is used as promotor is for analyzing its effect on the catalyst

properties in the Fischer-Tropsch synthesis. Its estimated capability of reducing the cobalt oxides at a lower temperature (Martinelli, et al. 2020) (Arsalanfar, et al. 2012) (Ernst, Hilaire and Kiennemann 1999) , influencing in the reaction selectivity (Guilera, et al. 2022), influence in CO₂'s reactivity (Martinelli, et al. 2020), make the cerium eligible as a candidate for optimizing the FTS.

For example, (Clarkson, et al. 2018), studies the effect of the ruthenium on the cobalt oxides, concluding that the Ru lowers the reduction temperature from T^o=[300-350°C] to T^o=[280-290°C] for cobalt(III) oxides and lowers the intervals from T^o=[400-800°C] to T^a[300-700°C] for the cobalt(II) oxide in its reduction to metallic cobalt.

Literature agrees that the Ceria affects the redox and electronic properties of the active phase, shaping a singular adsorption behavior reflected in the unusual catalytic features of the active phases, and enhances surface affinity for CO and H₂ molecules, as stated by (Martinelli, et al. 2020) (Mirzaei, et al. 2007). Some studies found the effect of ceria controversial because its effect on conversion is unclear, even though solid-state interactions and reactivity seem enhanced towards the gas phase (Mirzaei, et al. 2007). Nevertheless, Literature generally agrees on the positive effect of cerium oxide as a promoter (Guilera, et al. 2022). As for means, it is described that the Co-Ce matrix plays a synergistic role in the chemisorption of reactant molecules, because CeO₂ creates a CeO_x network that allows to capture oxygen, thereby controlling the reactivity of the FTS. Moreover, the cerium oxide has also shown an effect in lowering the conversion towards CH₄ and CO₂ (Zeng, et al. 2011), which are undesirable products in the Fischer-Tropsch Synthesis and increasing the conversion towards long-chain hydrocarbons (C₅₊).

2.4. Reaction:

Prior to the reaction, the catalyst is dissolved in SiC and loaded in the reactor (Davis 2005). The dilution of the catalyst is done in order to prevent the formation of hot spots (Aligolzadeh, et al. 2015) and avoid reactor's run-away (Fratalocchi, et al. 2020). (Berger, et al. 2002), advises that dilution may significantly reduce conversion due to local bypass effects, as seen in Figure 4, taken from their paper, in which at the left side of the figure, three fixed beds with different distribution of inert material are compared to their conversion, in the right side. In which the effect of these different distributions are compared to an irreversible first order reaction's conversion.

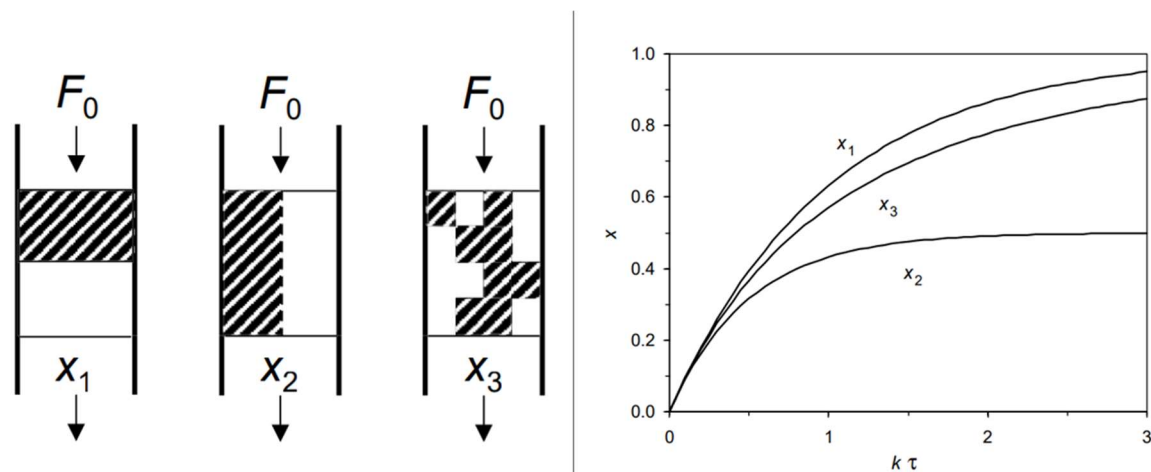


Figure 4: Effect of the dilution on fixed beds. Image taken from (Berger, et al. 2002)

Bed dilution does not yield a homogeneous activity decrease but gives rise to a discrete local activity in an inert surrounding. Excessive dilution can result in local bypassing, that results in deviations from the plug flow performance, especially at high conversions (Hickman, Degenstein and Ribeiro 2016). Distribution and transport mechanisms must not be belittled, due to their implications on product distribution, reactor performance, and staff safety.

Before reaction, reduction of the cobalt oxides is performed for obtaining metallic cobalt, because the metallic cobalt is the active phase of the reaction (Fratolocchi, et al. 2020, Ernst, Hilaire and Kiennemann 1999). According to literature it was thought that Cobalt could go through the same processes as iron catalysts to obtain carbides, oxides or even aggregates, when undergoing the reactions. Now it is widely accepted that cobalt has a lesser tendency to produce carbide than Fe catalysts, and that the active phase of the FTS is the metallic cobalt (Mirzaei, et al. 2007).

3. Objectives:

3.1. General Objective:

The main objective of this research study is to synthesize, to characterize and to perform catalytic reaction evaluations of materials for the conversion of syngas/CO₂ mixtures, with the aim to maximize the production of synthetic liquid fuels.

3.2. Specific Objectives:

- To perform a systematic study of the best conditions for the synthesis of γ -Al₂O₃ –supported cobalt catalysts for the FTS.
- To perform a complete characterization (physical properties, chemical composition, morphology, and surface characteristics) of the catalytic materials obtained.
- To analyze the correlation between the physicochemical properties of the catalysts, and their catalytic behavior in the FTS.
- To synthesize and to characterize CeO₂-promoted Co/ γ -Al₂O₃ catalysts.
- To evaluate the catalytic behavior of CeO₂-Co/ γ -Al₂O₃ catalysts in the FTS and in the FTS with syngas/CO₂ mixtures.
- To analyze the correlation among the synthesis, the physicochemical properties, and the reaction conditions for the synthesis of synthetic fuels in CO₂/syngas mixtures.

4. Methodology:

4.1. Impregnation:

The catalysts used in this investigation were obtained by the impregnation of a Cobalt(II) Nitrate hexahydrate, $[\text{Co}(\text{NO}_3)_2 \cdot 6 \text{H}_2\text{O}]$ (Honeywell, FLUKA TM, ACS Reagent $\geq 98\%$) or Cerium(III) nitrate hexahydrate, $[\text{Ce}(\text{NO}_3)_3 \cdot 6 \text{H}_2\text{O}]$ (Alfa Aesar, REacton[®], 99.5) solution over $\gamma\text{-Al}_2\text{O}_3$ spheres (Norpro Saint-Gobain, $\text{dp}=0.5 \text{ mm}$). The commercial γ -alumina was dried for at least 24 h at 105°C . The cobalt/cerium nitrate is dissolved in 4 times the total pore volume of the $\gamma\text{-Al}_2\text{O}_3$ pellets for each impregnation.

Once the cobalt nitrate solution is prepared, the impregnation over the $\gamma\text{-Al}_2\text{O}_3$ pellets was carried out with a syringe, for the dropwise addition. Note that the $\gamma\text{-Al}_2\text{O}_3$ pellets are white, and the solution of the $\text{Co}(\text{NO}_3)_2$ is pink/red (Figure 5). In a similar procedure, the Cerium(III) Nitrate is impregnated over the $\gamma\text{-Al}_2\text{O}_3$ spheres to yield a 9.6 wt.% over the $\gamma\text{-Al}_2\text{O}_3$ or $\text{Co}/\gamma\text{-Al}_2\text{O}_3$ support. Cerium(III) Nitrate is a translucent and colorless solid, that gives a transparent solution. After calcination, the $\gamma\text{-Al}_2\text{O}_3$ spheres turn yellow due to the presence of CeO_2 .



Figure 5: Left: Experimental setup for the synthesis of the catalysts. Right: $\text{Co}(\text{NO}_3)_2$ Impregnated $\gamma\text{-Al}_2\text{O}_3$ (before calcination).

After impregnation, the flask is put in a rotatory evaporator with moderate/high vacuum, water recirculation, and moderate agitation. The drying temperature is 80°C and is achieved by a bath of water-ethylene glycol solution while agitation is applied for assuring a good homogenization between the particles.



Figure 6: Left: Supported Cobalt Nitrate over γ -Al₂O₃, final product after the 2^o drying. Right: Supported Cobalt oxide over γ -Al₂O₃ after being calcinated at 500°C

A second drying is applied to remove the remaining moisture and facilitate the homogenization of the catalyst. Finally, the flask is removed, and the catalyst is collected for subsequent drying/calcination, as shown in Figure 6.

For calcination, the particles were subjected to heat treatment at two different final temperatures 275 °C, and 500 °C, with a ramp of 2°C/min. After the desired temperature is reached, a 5-hour dwell was performed to obtain the cobalt oxide.

A visual indicator that the nitrates have decomposed is that the catalyst turns black, see Figure 6. If the catalyst turns blue, that could mean a strong presence of CoAl₂O₄. (Małecka, et al. 2015).

4.2. Characterization of the Materials:

All samples were characterized by a series of techniques with the aim to correlate their structural and physicochemical properties and metal-support interactions with the activity results.

The experimental techniques used in this investigation are the following:

- **Temperature Programmed Reduction (TPR):** Micrometrics Autochem II equipment was used to study the reducibility of each sample at a programmed temperature. The sample is kept in contact with a 50 mL/min flow of 10 % H₂ (Ar balance), while it is subjected to a linear increase of the temperature in a 10°C/min rate, quantifying the amount of H₂ consumed as a function of the temperature.
For each analysis 0,1 g of each sample was weighed and placed in a U-shaped quartz reactor, supported on quartz wool.
- **X-Ray Diffraction (XRD):**, Is a technique that utilizes X-ray radiation on crystalline organic and inorganic samples. X-ray diffraction (XRD) measurements were performed on the catalysts using the Cu K radiation of a Bruker type XRD D8 Advance A25 diffractometer. The powder diffractograms of the samples were collected over a 2θ range of 10–70° at a step time of 1 s and

with a 0.002° 2θ spacing. XRD analyses allowed the identification of the cobalt phases present in the samples.

The identification of the phases was made with the X'Pert Highscore Plus V.2.0.1 Software. For calculating the size of the crystals, the Scherrer equation (1) was used:

$$L = \frac{K \lambda}{\beta \cos \theta} \quad [1]$$

Where:

- L is the mean size of the crystals;
 - K is the adimensional shape factor, whose value is 0.9;
 - λ is the X-ray wavelength, whose value is 0.154 nm;
 - β is the full width at half maximum (FWHM) angles, in radians. It can be represented as $\Delta(2\theta)$.
 - θ is the angle at which the maximum is achieved, known also as Bragg Angle, in radians.
- ***N₂ Adsorption:*** N₂-physisorption measurements were conducted in the TriStar II 3020-Micromeritics analyzer at liquid nitrogen temperature. Prior to the measurements, the samples were degassed at 90 °C for 1 h and then at 250 °C overnight in a FlowPrep 060-Micromeritics. The Brunauer–Emmett–Teller (BET) method was applied to calculate the BET surface area for a relative pressure (P/P₀) range of 0.05–0.3. The average pore size was determined by applying the Barrett–Joyner–Halenda (BJH) method to the desorption branch of the isotherms. The total pore volume was determined from the maximum adsorption value at P/P₀ = 0.997.
 - ***Scanning Electron Microscopy (SEM):*** Scanning electron microscopy (SEM) micrographs and elemental composition of the samples were obtained using a field emission scanning electron microscope (Zeiss Auriga 60) equipped with an energy-dispersive X-ray spectrometer (Oxford X-Max). For energy-dispersive X-ray (EDX) mapping, the catalysts were cold-drawn in epoxy resin and left to cure for 24 h. The epoxy molds were then polished to obtain the cross-section of the spheres and coated by gold sputtering.
With the Energy-Dispersive X-ray spectrometer, the elementary composition and presence can be measured of the catalyst particles. For this purpose, the catalyst particles are sanded until the equator of the particles is reached, and then, the catalyst particles are covered by a thin gold layer for the further analysis. The gold layer is added for favoring the conductivity of electrons through the catalyst particles.
 - ***ICP:*** ICP (Inductively Coupled Plasma) Spectroscopy is an analytical technique used to measure and identify elements within a sample matrix based on the ionization of the elements within the sample. Mass Spectrometer (MS) separates the ions by their mass-to-charge ratio after going through the ICP, and the detector counts the number of selected ions per second which allows

the instrument to determine the concentration of each chosen element. (OHSU 2023)

- **CO Chemisorption:** Is a technique used to determine the metallic surface area and the dispersion of the metal in the sample. Measurements were conducted in a Micrometrics Autochem II equipment by pulsed CO chemisorption, prior to adsorption measurements, samples were reduced in H₂ flow at 500°C.
- **Density:** The real density of the samples was measured by Quantachrome Micro Ultrapyc 1200e Automatic Gas Pycnometer, a helium pycnometer. With this apparatus, the real density is estimated by passing helium at 20 psig pressure to the sample. Three measurements were performed, for obtaining the average values.
Apparent density was estimated by weighting different volume of the samples in a test tube.

4.3. Reaction

4.3.1. Setup:

The reaction was carried out in a fixed bed plug flow reactor, Microactivity model of PID Eng&Tech. The reactor consists of a tubular stainless-steel pipe of 13 mm diameter and 305 mm length, that is placed inside a ceramic chamber, heated by an electrical resistance. The temperature inside the reactor was measured by a type K thermocouple inserted into the catalytic bed and was controlled by a digital PID controller. A scheme of the process is depicted in Figure 7.

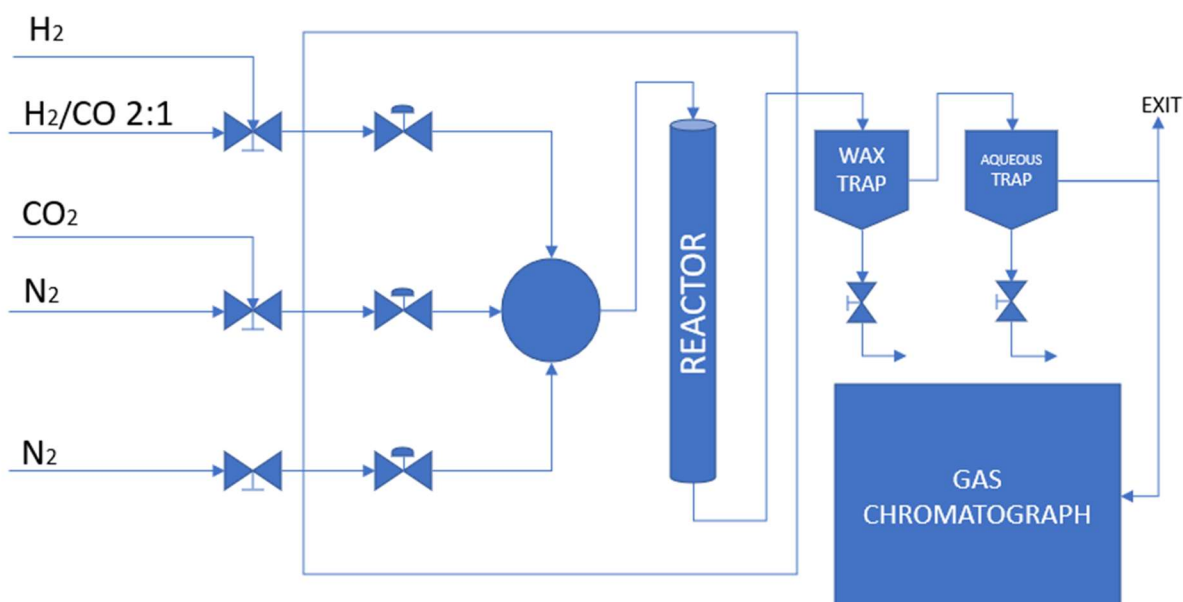


Figure 7: Diagram of the reaction system.

The inlet gases enter via 3 different channels equipped with mass flow controllers. The gases used were: 2:1 H₂/CO Syngas mixture; pure hydrogen; Nitrogen; and CO₂. The exit flow passed through a wax trap for the condensation of liquids and waxes at 20 bar·g and 100°C. The exiting gas then flows to the “aqueous trap”, in which water and other light organic chemicals condense at 100°C and 20 bar·g.

The residual gas is then sent to the Gas Chromatograph (GC), a micro-chromatograph Agilent Technologies 490 Micro GC Biogas Analyzer model. The GC is composed of three channels, the first channel, with a MS5A column, was used for the analysis of H₂, N₂, CO and CH₄; the second channel, using a PPQ column, was used for the analysis of CO₂, C2 and C3; and the third channel, an Al₂O₃ column was used for the analysis of propane, propylene, and butane. The carrier gas in all channels was Helium.

4.3.2. Procedure:

The preparation of the fixed bed is carried out by weighting the catalyst and then mixing it to a 1:10 ratio with silicon carbide (SiC, Alfa Aesar). This dissolution is performed in order to achieve a good heat transfer and assure isothermicity.

Before the reaction, a leak test was performed. For each leak test, nitrogen is introduced in the reactor until the pressure reaches 30 Bar, and a pressure drop lower than 0.1 bar/min is reached. For measuring this rate, the nitrogen flow is cut, and pressure fall is measured. The minimal time for the leak test is 30 min. After the leak test, the reduction of the catalysts was performed with a hydrogen (pure) flow of 95 NmL H₂/min. The reduction is carried out in three steps; in the first stage, the reactor line is pre-heated during 4 hours to 120°C to unplug and clean the reactor from residual waxes; In the second stage the reactor is then heated to 380°C at a 0.5°C/min rate for 11 hours; and finally the reactor is cooled to 160°C with a H₂ flow of 46 NmL/min during 9 hours.

4.3.3. Catalytic Test:

Reaction conditions varied in function of the research stage, hereunder investigation stages are described:

- **1^o Stage:** The aim of this stage is to optimize the synthesis of the catalyst and to study the influence of the working variables on the catalytic behavior of the material. For this purpose, we worked at a constant temperature of 230°C and at three different syngas flows [$F_{\text{syngas}} = 140 ; 70 ; 35$] cm³/min.
- **2^o Stage:** In this stage, the working conditions were different, since the aim was to keep the conversion constant, by changing the inlet flows, in order to compare the performance of the catalysts (selectivity) and to study the influence of temperature on the distribution of the products and reactants.

Below is a scheme illustrating the planning followed during this research. In blue, the first phase corresponds to the optimization of the synthesis condition of the Co/ γ -Al₂O₃ catalysts. Once the optimized methodology for the synthesis of Co/ γ -Al₂O₃ catalysts was selected, the second stage of this research analyzed the effect of the addition of cerium oxide. The cerium-promoted catalysts are then tested under CO₂-free syngas and under a CO₂-rich syngas mixture. The second phase of the research is highlighted in yellow.

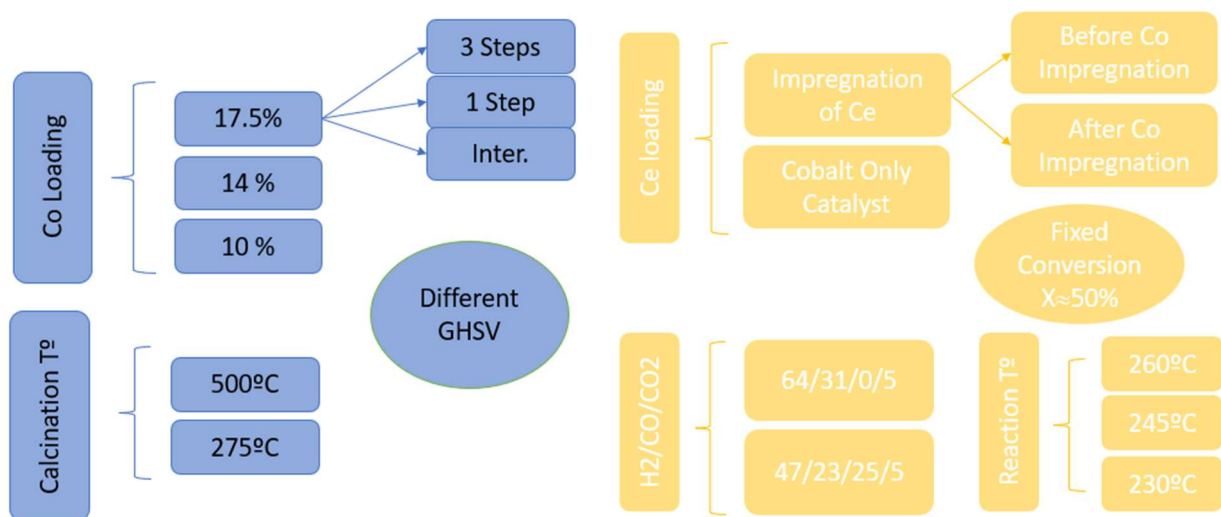


Figure 8: Experimental design.

The series of catalysts samples obtained are described in Table 2. A brief description of the procedural parameters such as the composition (nominal), calcination temperature (A = Calcination temperature of 500 °C; B = Calcination temperature of 275 °C) and number of impregnation steps of the catalysts. The catalysts were synthesized to achieve a nominal metallic loading of wt% = [10%;14%;17.5%]. All catalysts described in Table 2, were prepared by impregnating Co(NO₃)₃·6H₂O and Ce(NO₃)₃·6H₂O over γ -Al₂O₃.

Table 2: Description of the catalysts: Composition and procedural parameters.

ID	Description
10A	10 wt% cobalt supported over γ -Al ₂ O ₃ calcined at 500°C.
10B	10 wt% cobalt supported over γ -Al ₂ O ₃ calcined at 275°C.
14B	14 wt% cobalt supported over γ -Al ₂ O ₃ calcined at 275°C.
14A	14 wt% cobalt supported over γ -Al ₂ O ₃ calcined at 500°C.
17.5A1	17.5 wt% cobalt supported over γ -Al ₂ O ₃ calcined at 500°C and impregnated in one step.
17.5A3	17.5 wt% cobalt supported over γ -Al ₂ O ₃ calcined at 500°C and impregnated in 3 steps.

17.5Bi	17.5 wt% cobalt supported over γ -Al ₂ O ₃ calcined at 275°C, impregnated in 3 steps with intermediate calcination between every impregnation.
17.5B1	17.5 wt% cobalt supported over γ -Al ₂ O ₃ calcined at 275°C impregnated in one step.
Co/ γ -Al ₂ O ₃	17.5 wt% cobalt supported over γ -Al ₂ O ₃ calcined at 275°C impregnated in one step.
Ce/Co/ γ -Al ₂ O ₃	8.5 wt% Cerium impregnated over a 17.5 wt% Co/ γ -Al ₂ O ₃ catalyst.
Co/Ce/ γ -Al ₂ O ₃	17.5 wt% Cobalt impregnated over a 8.5 wt% Ce/ γ -Al ₂ O ₃ catalyst.

4.3.4. Calculations:

The reaction parameters were determined by the following equations:

$$n_{Tot,ent} = \frac{PV}{RT} \quad [2]$$

The molar flows were calculated at standard temperature and pressure condition (STP): T = 273 K; P = 1 atm; V = Inlet flow, mL/min. For estimating the molar flow for each substance, the calibration curve for each compound is used. For calculating the inlet flow, $n_{i,ent}$, the for reaction, obtaining the following equation:

$$n_{i,ent} = \frac{n_{Tot,ent} \times \%[i]_{ent}}{100} \quad [3]$$

Where $\%[i]_{ent}$ represents the molar percentage of the substance i in the mixture measured by the GC.

For the estimation of the molar flows of the outlet gases, the following equations are used:

$$n_{N_2,ent} = \frac{n_{Tot,ent} \times A_{N_2,ent}}{100} \quad [4]$$

Where, $A_{N_2,ent}$, represents the area of the N₂ measured in the GC. Nitrogen is used as a internal standard.

$$n_{Tot,exit} = \frac{n_{N_2,ent} \times 100}{A_{N_2,exit}} = \frac{n_{Tot,ent} \times A_{N_2,ent}}{A_{N_2,exit}} \quad [5]$$

With the entering and exiting N₂ areas a correlation of moles exiting the system in gaseous form can be established. With the total moles exiting the system quantified, the molar flows of each component can easily be calculated as:

$$n_{i,exit} = \frac{n_{Tot,exit} \times \%[i]_{exit}}{100} \quad [6]$$

Where $\%[i]_{exit}$ represents the molar percentage of the substance i in the mixture measured by the GC, as in equation [3].

The conversion is calculated using equation 7 and is applied to CO; H₂; and CO₂.

$$\%Conversion_i = \frac{n_{i,ent} - n_{i,exit}}{n_{i,ent}} \times 100 \quad [7]$$

The selectivity of the gaseous products (C1-C4, CO₂) is calculated using equation 7, where C_i is the number of carbons in the i molecule.

$$\%Selectivity_i = \frac{C_i \times n_{i,exit}}{n_{CO,ent} + n_{CO_2,ent} - (n_{CO,exit} + n_{CO_2,exit})} \times 100 \quad [8]$$

$$\%Selectivity_{C_{5+}} = 100 - \sum_{i=1}^{n=4} \%Selectivity_i \quad [9]$$

5. Results:

5.1. Characterization:

5.1.1. Density and ICP%:

The chemical composition determined by the ICP-AES was lower than the expected nominal values. Samples were synthesized for the following composition wt%= [10% ;14%; 17.5%]. Promoted samples were prepared with a nominal fixed cerium content of 10 wt%. The experimental weight percentages are shown in Table 3.

The most notable difference between the nominal values and the ones obtained by ICP-AES are between the catalyst with a nominal value of cobalt loading of 14%, and more specifically for the catalyst 14B, for which the relative and absolute error are 23% and 3.20 [%].

Table 3: Physical (density) properties and chemical composition of the synthesized catalysts.

Name	Wt%ICP Cobalt	Real Density [kg/ dm ³]	Aparent Density [kg/ dm ³]
10A	9.20	3.28	0.645
10B	8.60	3.27	0.655
14B	10.80	3.33	0.655
14A	11.55	3.35	0.655
17.5A1	16.00	3.46	0.653
17.5A3	15.40	-	-
17.5Bi	14.65	3.39	0.676
17.5B1	15.20	3.43	0.652
Co/ γ -Al ₂ O ₃	14.3*	3.50	0.665
Ce/Co/ γ -Al ₂ O ₃	15.27(9.37*)	3.67	0.653
Co/Ce/ γ -Al ₂ O ₃	14.5(9.43*)	3.49	0.645
γ -Al ₂ O ₃	0	3.27	0.655

*Wt% of Cerium estimated by EDX

For the non-promoted catalysts, a correlation can be found between the density and the loading of the metal in the catalyst, as shown in Figure 9.

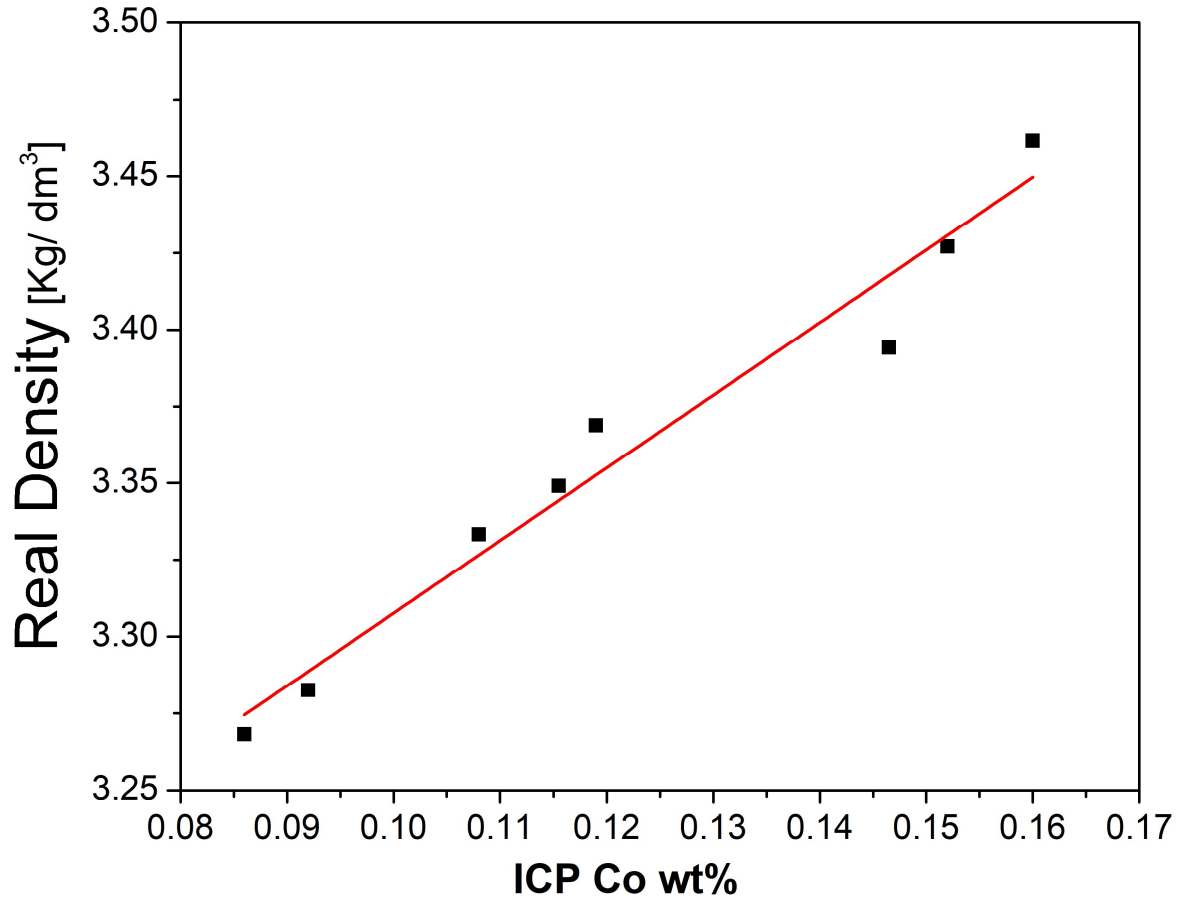


Figure 9: Correlation of the real density and the cobalt loading.

In Figure 9, a relation can be determined between the real density and the wt% Co loading estimated by the ICP-AES. A linear fit ($a+bx$) is performed, and the obtained values are presented in the next equation: $3.07 + 2.37 \cdot Co$ (Co %wt presented as per one). From the values obtained a R-square of 0.96 is obtained implying a good correlation between the wt% of Co estimated by the ICP-AES and the real density measured by the pycnometer. This data is congruent due to the higher density of the cobalt oxides in comparison to the density of the $\gamma\text{-Al}_2\text{O}_3$.

5.1.2. SEM

The scanning electron microscopy allows appreciating the morphology of the catalyst particles. In figure 10, the particle and its surface morphology at a 40K magnification is observed.

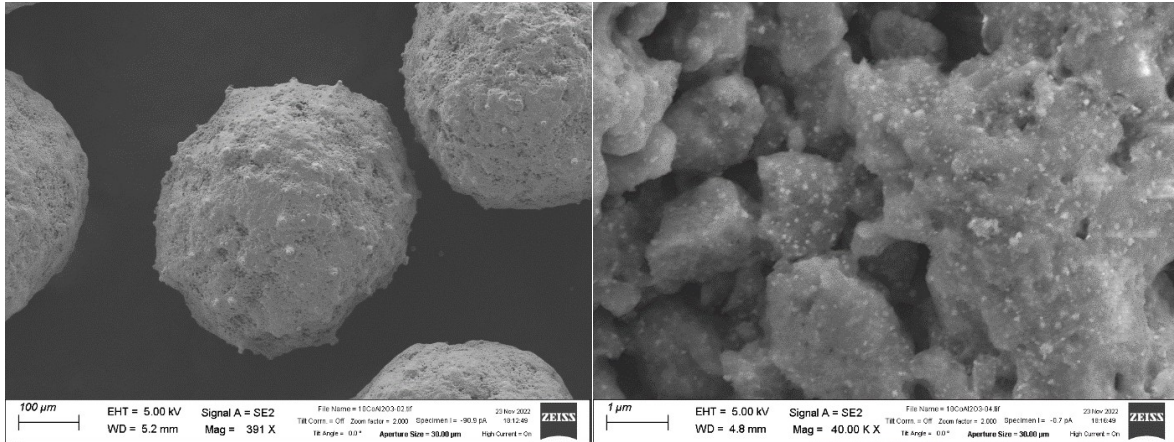


Figure 10: SEM image of the 10A Catalyst pellet.

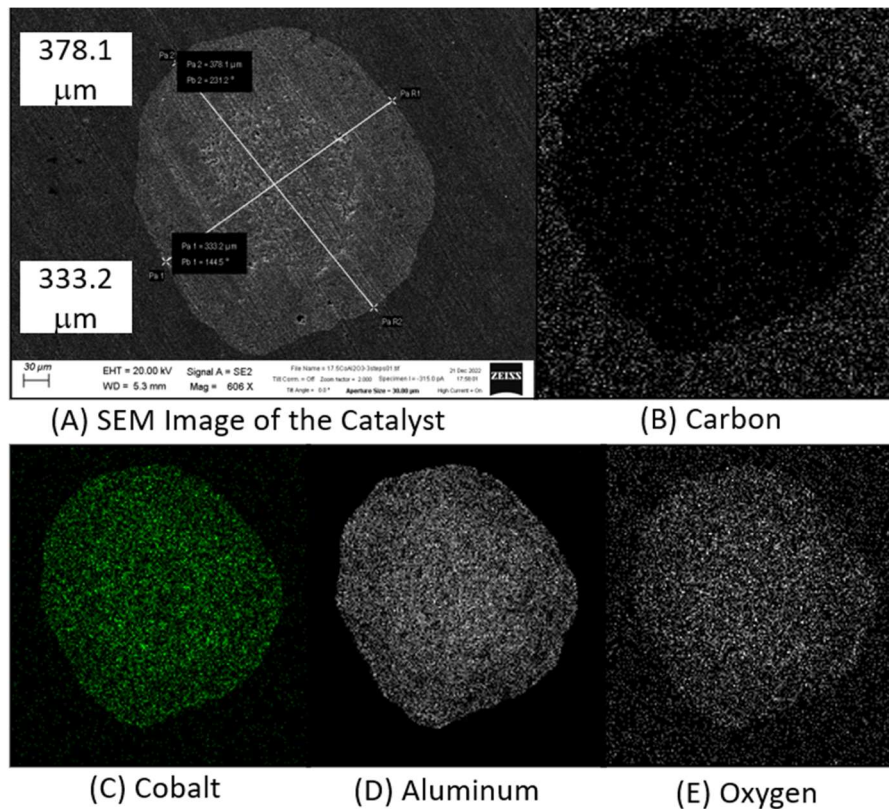


Figure 11: Cross-section of a catalysts particle (17.5A3)(A) SEM micrography of the particle; (B) EDX of Carbon atoms; (C) EDX of cobalt; (D) EDX of Aluminum atoms; (E) EDX of oxygen.

From figure 11, we observe that the impregnated cobalt is evenly distributed along the catalyst particle. Note that the points represent the cobalt presence not the particle size.

5.1.3. N₂ Adsorption:

N₂ adsorption is a technique that allows calculating, via different methods, these parameters: Surface Area; Pore Volume; and Pore Size. Surface area is a crucial parameter for optimizing the use of porous materials in many applications. Due to the complex nature of micro/mesoporous materials, no single experimental technique can be expected to provide an evaluation of the absolute surface area, however, the most frequently applied method is the BET method introduced by Brunauer, Emmett, and Teller (Thommes 2010).

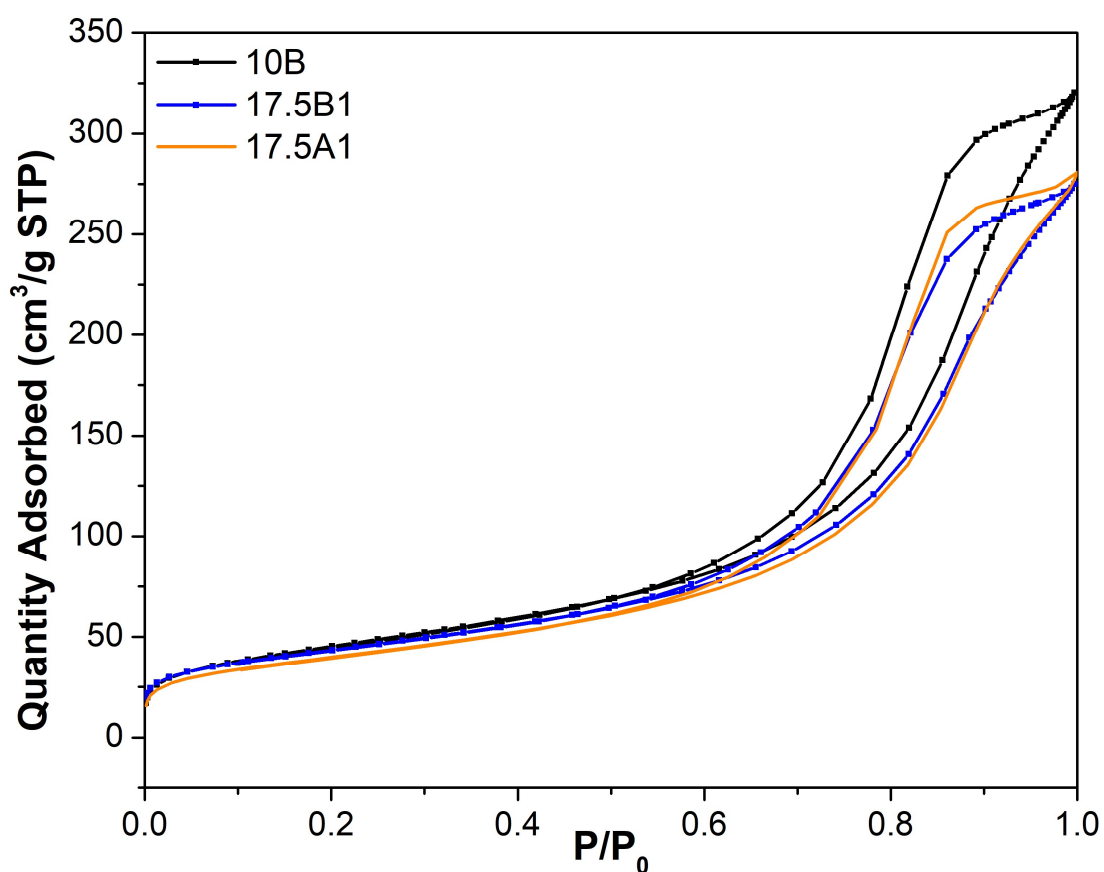


Figure 12: Isotherms of the catalysts.

According to IUPAC's isotherm classification (Thommes, et al. 2015), the shape of the adsorption-desorption isotherms obtained in Figure 12, correspond to a type IV(a) isotherm and a H2(b) hysteresis loop. Type IV(a) isotherms are typical of mesoporous adsorbents.

Table 4: N₂ Adsorption parameters

ID	S _{BET} (m ² /g)	V _{meso} (cm ³ /g)	V _{micro} (cm ³ /g)	S _{ext} (m ² /g)
10A	152	0.48	0.0015	145
10B	176	0.52	0.0026	160
14B	161	0.50	0.0049	153
14A	150	0.49	0.0023	147
17.5A1	144	0.45	0.0007	140
17.5A3	162	0.49	0.0008	157
17.5Bi	168	0.49	0.0025	160
17.5B1	151	0.44	0.0023	147

The data shown in Table 4 shows that the methodology of preparation has an effect on the surface area of the catalysts, for instance, it is observed that a higher calcination temperature gives a lower surface area (Fratolocchi, et al. 2020), mainly because of the sintering of the cobalt oxide particles. It can be also noted that 17.5A3 catalyst gives higher surface area than the 17.5A1 catalyst. However, when comparing the 17.5Bi and the 17.5B1 catalyst, similar effect on S_{BET} is detected.

Another factor that influences the S_{BET} is the Co loading. The higher the Co loading, the lower the S_{BET}. This behavior can be explained because the cobalt oxide is not a porous solid, thus leading to a global decrease in the surface area. The highest area [S_{BET}=176 m²/g] is obtained by the 10% cobalt-loaded catalyst calcined at 275°C; and the lowest area [S_{BET}=144 m²/g] is obtained by the 17.5% Cobalt-loaded catalyst calcined at 500°C impregnated in one step. Same conclusion can be applied to the external surface. This is congruent with (Clarkson, et al. 2018) observations, in which they indicate that at more impregnation steps the lower the sintering. From the results obtained this conclusion can be affirmed for the 17.5A3 catalyst in comparison with the 17.5A1 catalyst.

The mesopore volume behaves differently from the BET area and the external surface, for instance, it is true that the highest mesopore volume is obtained with the 10% cobalt-loaded catalyst calcined at 275°C [V_{meso}=0.515 (cm³/g)]; nevertheless, the lowest mesopore volume is obtained with the 17.5% Cobalt-loaded catalyst calcined at 275°C [V_{meso}=0.439 (cm³/g)]. No clear tendency is seen in the experimental data for the mesoporous volume. The volume of micropores is minimal, implying that the catalysts are mainly mesoporous.

In Figure 13, the distribution of the pores is represented. For all catalysts, the pore distribution is similar. As observed in table 4, the volume of micropores is negligible. Thus, being congruent with the classification and shape of the isotherms (Figure 12). The other parameters are calculated by the Barrett-Joyner-Halenda (BJH) approach, for determining the pore volume; and the t-plot, to determine the external surface and micropore volume.

The BJH method has been used to create pore volume and surface area distributions based on a complete desorption or adsorption isotherm (Micromeritics n.d.). For instance, the adsorption capacity is dependent on the magnitude of the external area and on the upper limit of the pore size distribution. (Rouquerol, Rouquerol and Sing 1999)

The t-plot is based on the Kelvin equation and is obtained by representing the adsorbed volume respectively to the statistical thickness, instead of the relative pressure. The t-plot is useful for giving insight on the structure of the catalyst by detecting the presence of micropores by showing a deviation to the standard behavior. (Gregg and Sing 1982).

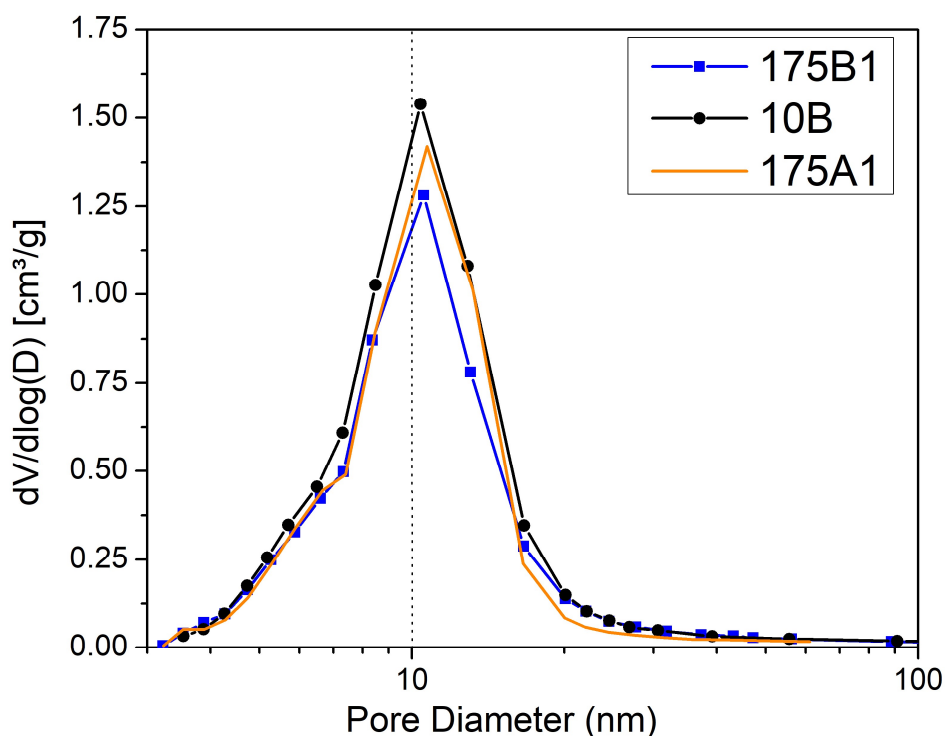


Figure 13: Pore Distribution of the 17.5B1, 10B and 17.5A1 catalysts.

5.1.4. XRD

The X-Ray Diffraction technique is used for determining the grain size of crystalline phases present in a material. This technique is particularly useful for determining, in a qualitative way, the presence of crystalline phases. Also, this technique, in assistance of Scherrer's equation, is helpful in determining the crystalline domine, and in some cases, the grain size, of the polycrystalline material.

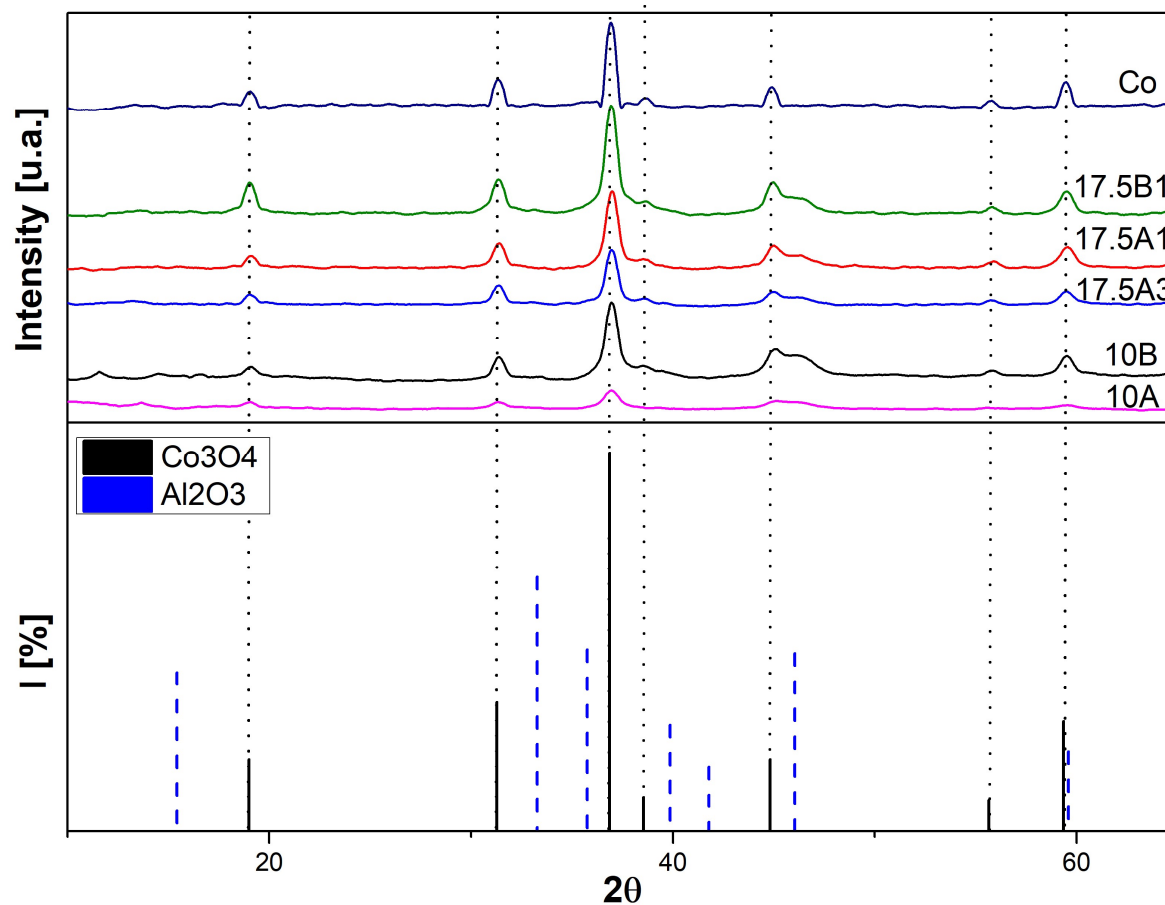


Figure 14: XRD of the non-promoted catalysts

In Figure 14, the measured signal for each catalyst is plotted respective to 2θ . The signal is analyzed in the X'Pert software for determining the crystalline phases present. The X'Pert software analyzes the peaks and compares them to other substance's peaks. Note that the Co_3O_4 and Al_2O_3 patterns have been selected because they are the most consistent considering catalysts' composition (non-promoted).

Table 5: Scherrer equation parameters and Crystalline Size

ID	FWMH (°)	D (nm)
10A	0.77	11
10B	1.02	8
14B	1.03	8
14A	0.89	9
17.5A1	0.72	12
17.5A3	0.75	11
17.5Bi	0.82	10
17.51	0.96	9

Co/ γ -Al ₂ O ₃	0.77	11
Ce/Co/ γ -Al ₂ O ₃	0.79	11
Co/Ce/ γ -Al ₂ O ₃	0.79	11

Also, for each catalyst, the crystalline size is measured by Scherrer's equation, by taking in account the main peak at 36.9°. The FWHM and the Crystalline size are presented in Table 5. Crystalline cobalt oxide sizes estimated by Scherrer's equation are similar for all catalysts and are estimated at 11 nm (table 5).

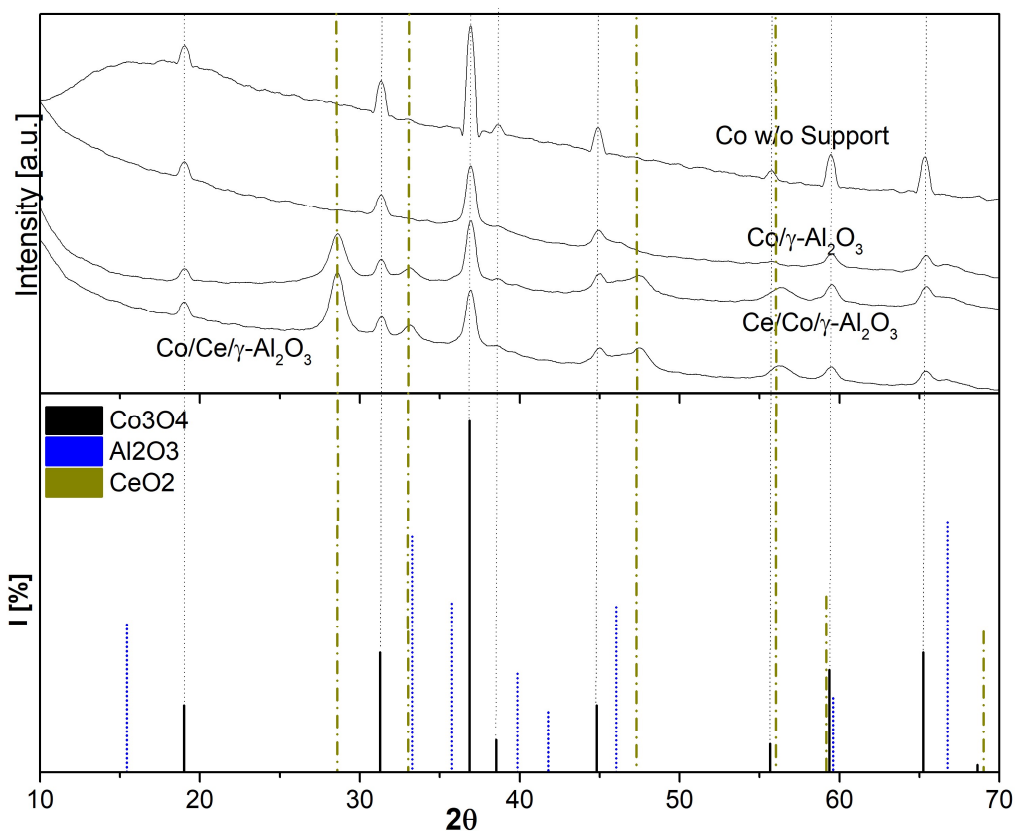


Figure 15: XRD of the Ce-promoted catalysts.

In Figure 14, the non-promoted catalysts were represented and compared to the XRD patterns of Co₃O₄ and Al₂O₃, while in Figure 15, the Ce-promoted catalysts were analyzed and studied in comparison with the above-mentioned patterns in addition to a CeO₂ pattern. Figure 15 shows that the difference, for the used 2 θ range, between the Ce-promoted and unpromoted catalysts can be summarized in 4 peaks, located at [29°; 33°; 47°; 56°].

Particle size of the cobalt oxides and its metallic form are crucial for the catalyst behavior, for instance, a low particle size leads to fast catalyst inactivation, another problem with small oxides is that they tend to react with the alumina support forming an irreducible species (CoAl₂O₄) that leads to metallic surface area loss. In the other hand, having large metallic particles leads to a lower dispersion of the metal in the support's surface. For example, (Bezemer, et al. 2006) (Borg, et al. 2007) determine that a metallic particle

size below 6 nm leads to rapid deactivation and rapid active surface loss in the catalyst, whereas oxide particles above 30 nm led to a conversion loss due a poor dispersion (Iglesia 1997).

5.1.5. TPR

The Temperature programmed reduction is used for the determination of the metallic species present in the reduction. For instance, (Clarkson, et al. 2018) points the ranges in which reduction of the cobalt oxides happen.

- a) Temperature [230-250°C]: This range corresponds to the reduction of the residual nitrates that were not completely decomposed during calcination. When using calcination temperatures higher than 275 °C (e.g. 500°C), these species do not appear.
- b) Temperature [300-350°C]: In this range, the reduction of the Co(III) to Co(II) transcur. This reduction can be written as follows:



- c) Temperature [400-800°C]: This range is where the cobalt oxides turn into metallic cobalt, nevertheless, if the temperature is high enough, formation of CoAl_2O_4 can happen. The Cobalt aluminate is a stable species that is irreducible and that doesn't participate in the Fischer-Tropsch Synthesis.



The cobalt aluminate formation is a spontaneous reaction when contact between the metallic cobalt and the $\gamma\text{-Al}_2\text{O}_3$ support is favored in a high temperature medium. (van de Loosdrecht, et al. 1997), indicates that small cobalt oxide tends to react to form the aluminates.

In this work, samples of the supported catalysts; and a sample of the cobalt oxide prepared without the support; were analyzed in order to study the influence and correlation between them and their response to the reduction conditions. For instance, in Figure 16, the reduction of the non-supported cobalt oxides was analyzed after ongoing thermal treatment (Calcination at 500°C), for determining the behavior of the cobalt catalyst without the influence of the $\gamma\text{-Al}_2\text{O}_3$.

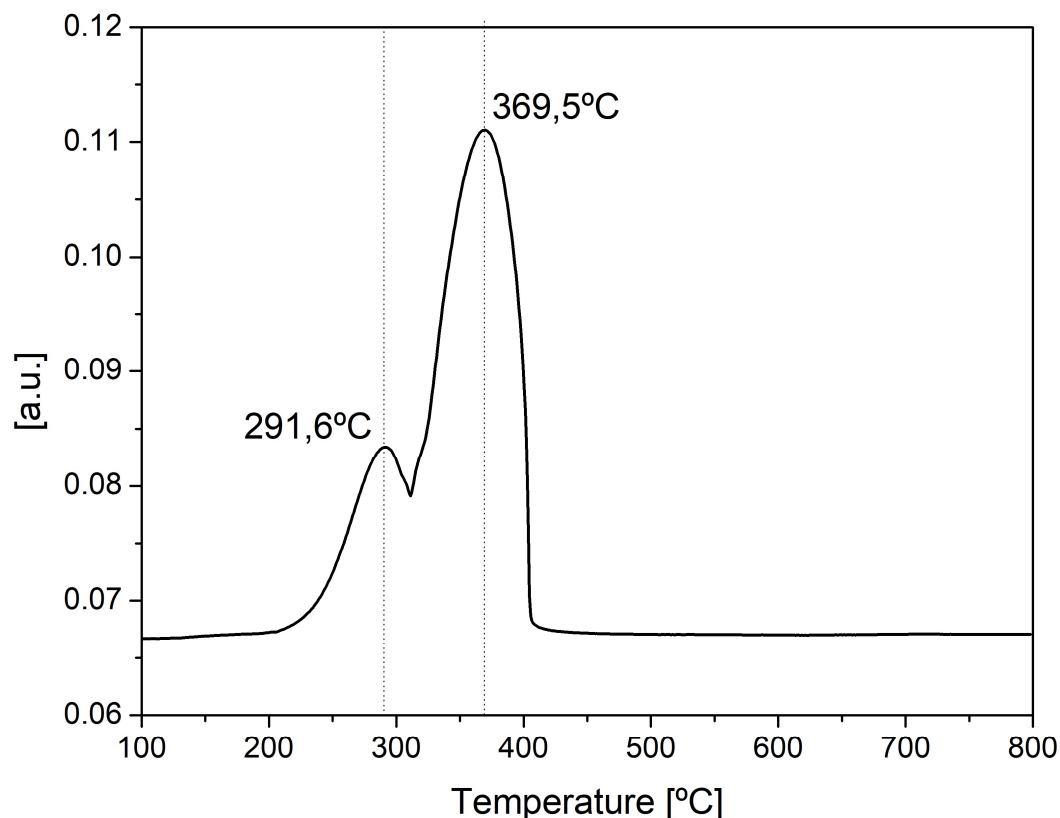


Figure 16:TPR profile of the non-supported cobalt oxide calcined at 500°C.

Figure 16 shows the main peaks of the unsupported cobalt oxide. For instance, it can be seen that the main peaks correspond to; $[T^{\circ}=291.6^{\circ}\text{C}]$ which is the reduction temperature of the Co(III) oxides; and $[T^{\circ}=369.5^{\circ}\text{C}]$ that is the reduction temperature of the Co(II) oxides. Both temperatures are below the ranges defined by (Clarkson, et al. 2018). Another observation is that the area below the Co(II) peak [Temperature= 369.5°C] is three times the area below the peak of the Co(III). This corresponds to the stoichiometry needed for the reduction of the oxides, revealing that effectively, these peaks correspond to the Co(III) and the Co(II) oxides as described.

When comparing the pure cobalt oxide to the supported cobalt catalysts, see Figure 17, it can be stated that the reduction temperatures obtained for the supported catalyst is lower than for the non-supported catalyst. This is due to the lower particle size (Clarkson, et al. 2018), when working with a support the cobalt particles tend to disperse on the support's surface area in comparison to the bulk oxide. A lower reduction temperature for the supported catalysts is also in agreement with the Hüttig and Tamman (Zhang, et al. 2011) temperatures, in which the surface and bulk atoms become mobile, respectively. A lower particle size implies lower reduction time as equilibrium is reached sooner under the same conditions.

Below a figure with the TPR figures of the cobalt oxides is indexed:

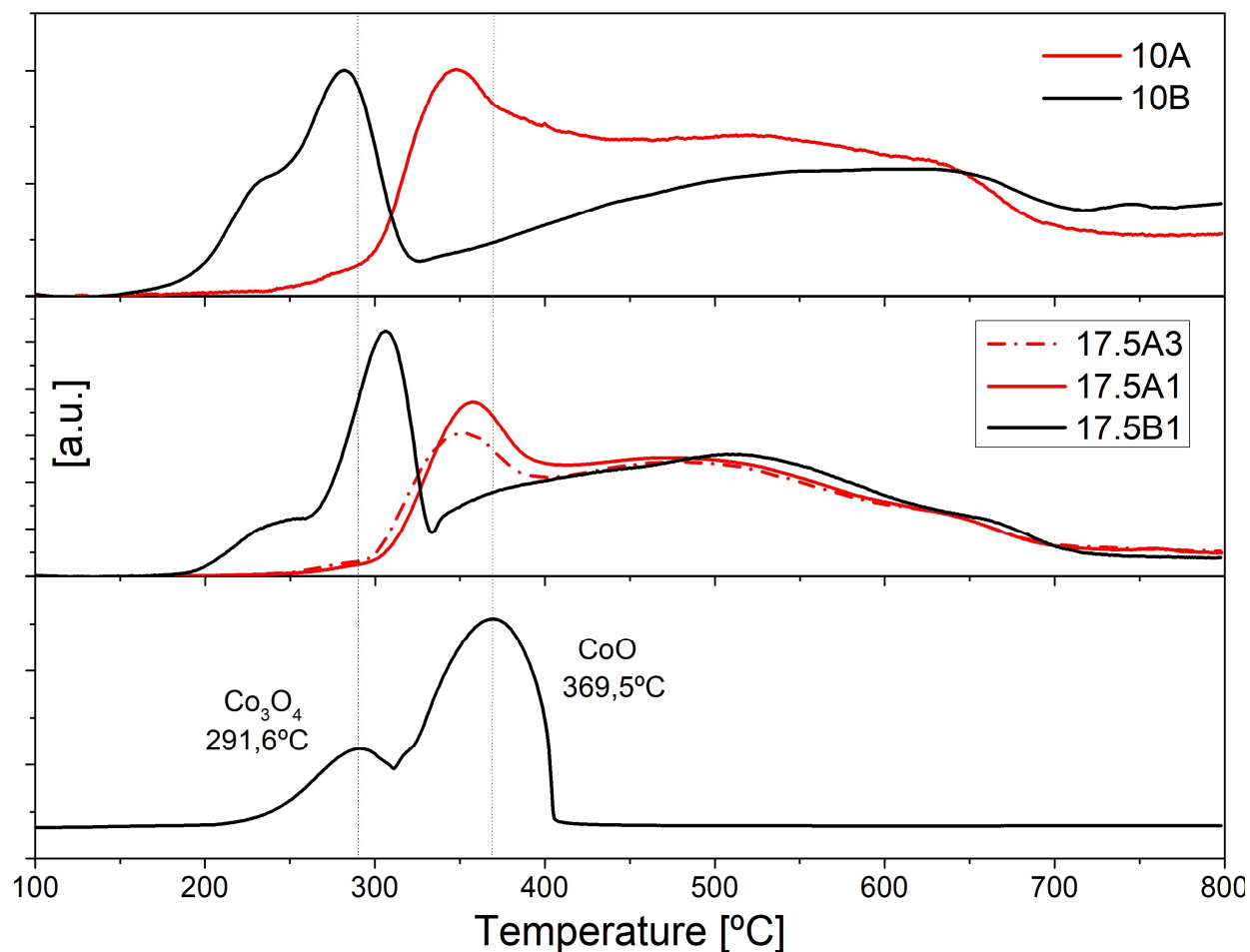


Figure 17: Comparison of catalysts' TPR

Figure 17 represents the TPR profiles of the catalysts used in this research. The catalysts were grouped in function of their nominal cobalt loading for the sake of clarity. In Figure 17, the difference between the calcination temperatures can be seen by reaching a reduction peak earlier. This effect can be seen for nominal cobalt loading of 10 wt% and 17.5 wt, by exception of the 17.5B1 catalyst, that reaches its reduction peak at higher temperature, implying a larger cobalt size. For the supported catalysts a hump can be seen for the temperature range of $T=[400-700^{\circ}\text{C}]$, in contrast with the pure cobalt oxide, this hump can be explained due to the interaction of the cobalt oxides with the $\gamma\text{-Al}_2\text{O}_3$ support (Fratalocchi, et al. 2020). No conclusion can be drawn from the TPR results between different compositions.

5.1.6. CO Chemisorption:

The CO Chemisorption is a technique that determines: the metallic surface area of the catalysts and the percent dispersion based on monoxide's ability to chemisorb on the cobalt's surface. These parameters are determined by measuring the difference between CO concentration between the different injections.

The values calculated by the CO Chemisorption for the Ce-promoted catalysts are shown in Table 6, while the non-promoted catalysts' values are plotted in Figure 18.

Table 6: CO Chemisorption values

ID	Metal Dispersion[%]	Metallic Surface Area [m ² / g-sample]
Co	1.6	1.3
CoCe	1.3	1.1
CeCo	1.8	1.5

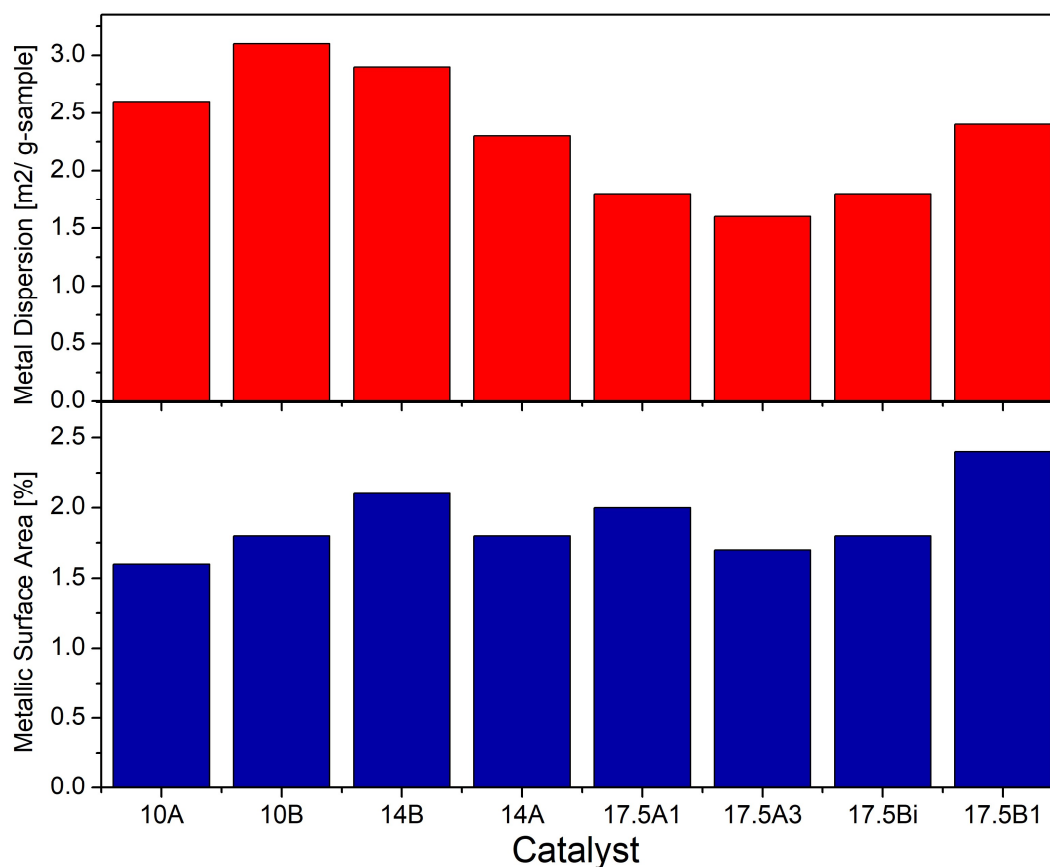


Figure 18: Metallic Surface Area and Metallic Dispersion measured by CO Chemisorption

The highest metallic surface area is obtained for the 17.5B1 catalyst, that contains a 17.5% nominal cobalt loading, obtained by unique impregnation and calcinated at 275°C. The metallic surface area tends to increase by lowering the calcination temperature and with higher cobalt loadings. A lower calcination temperature leads to a higher metallic dispersion for all nominal cobalt loading whilst decreasing with the nominal cobalt loading.

5.1.7. Main Findings

The chosen variables for the synthesis of Co/Al₂O₃ catalysts have an effect on their physicochemical properties. The main findings reached are that working at low calcination temperature and direct impregnation give improved results for every parameter studied, or at least, similar values were obtained as for the higher calcination temperature.

For instance, the main reason to vary the calcination temperature was to study if a calcination temperature of 275°C was enough to guarantee a nitrate decomposition, as detailed in chapter 3.5. TPR, and even if nitrate residues were still observable at 275°C, the results caused by the calcination the temperature on the above-mentioned parameters justify a calcination at lower temperature instead of 500°C. The effect of multiple impregnations was either negligible or worse than the effect of a unique impregnation. The nominal cobalt loading had a major effect on the catalyst's parameters, but the main question regarding the nominal cobalt loading, whether is it too much or adding more catalyst can still improve the results, is still unanswered until catalytic testing is performed. Note that these conclusions are preliminary. Catalytic testing must still be performed for analyzing the role of these.

5.2. Reaction:

Reactions were carried out in a fixed-bed reactor in different steps, for the unpromoted catalysts, the GHSV have been changed to study the behavior of the catalysts at different flows while for the Ce-promoted catalysts, temperature has been the main variable changed in the catalytic tests.

5.2.1. Optimization of the Cobalt catalysts:

For the optimization of the supported cobalt catalyst, catalysts were tested under FTS. During the reaction, different flows are studied to analyze the behavior of the catalyst at different conversions and selectivity, finally a comparison of catalysts productivity is shown and briefly discussed.

Conversion:

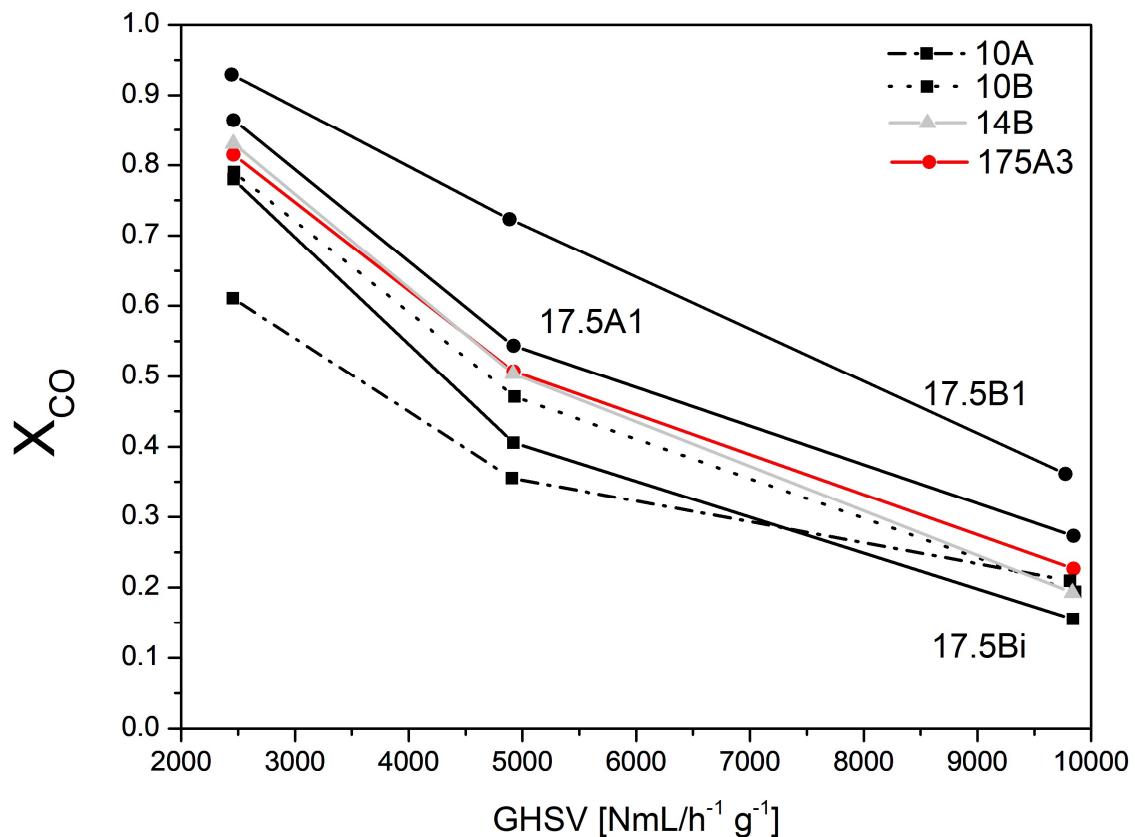


Figure 19: CO Conversion of the catalyst at different GHSVs

In Figure 19, the conversion of carbon monoxide is displayed alongside the GHSV. This figure shows that the conversion diminishes with the increase of GHSV. Also Figure 19 helps determining the most active catalysts. Generally, it is observed that at higher calcination temperature, a lower conversion is achieved.

Also, a higher Co loading seems to indicate a higher activity for the same conditions. Alongside the monoxide conversion, the hydrogen conversion is also needed for determining the catalysts conversion, especially for determining if other side reactions are participative in the process.

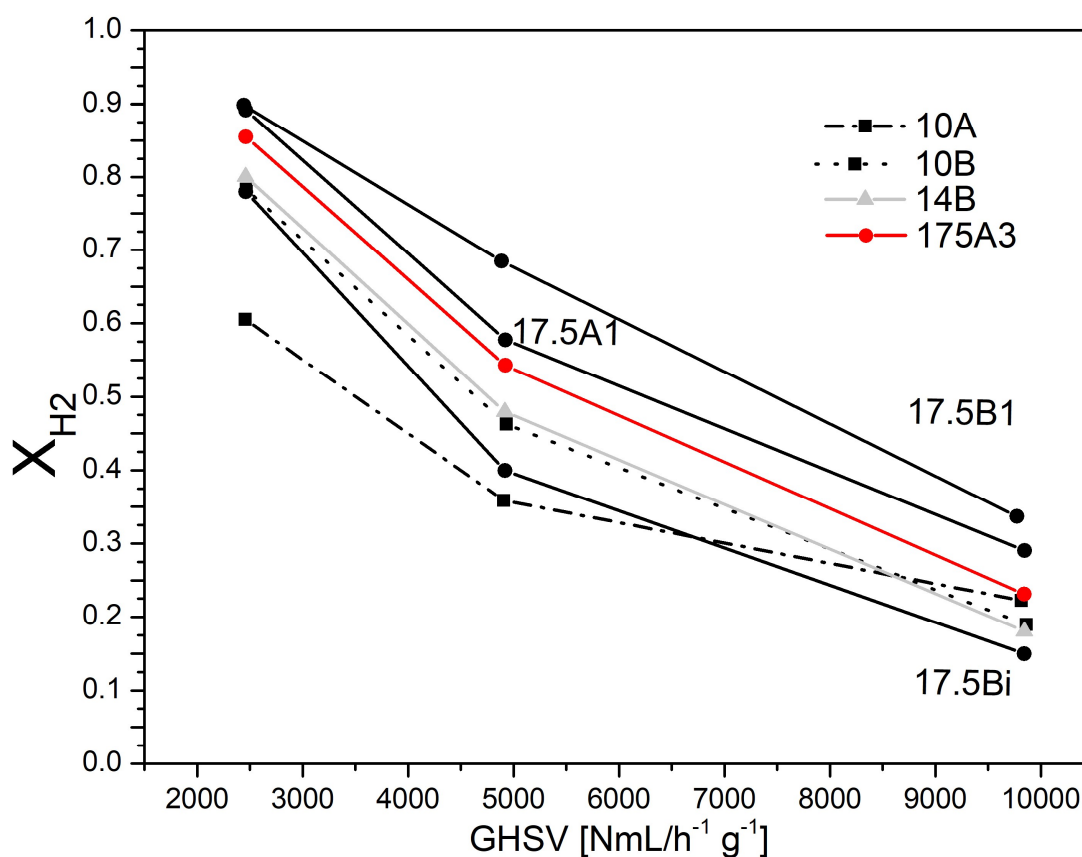


Figure 20: H₂ Conversion of the catalysts at different GHSVs.

In Figure 20, the hydrogen conversion is displayed, similar conversions of the reactants (Carbon monoxide and hydrogen) can be appreciated. In both figures, the most reactive catalyst is the 17.5 wt% Co obtained with a unique impregnation and low temperature calcination (17.5B1). This is congruent with the results obtained in the characterization chapter, in which, a lower calcination temperature and unique impregnation led to improved characteristics, such as a higher metallic surface area. The main concern from the characterization chapter was determining if Co loading was excessive or if, on the contrary, nominal Co loading could increase. Now, results show that the highest Co loading gives the highest conversion.

Even if conversion seems the most important factor for a reaction, it is not, remember that the FTS is a polymerization reaction, and that the objective is to obtain the highest quantity of C₅+ hydrocarbons. Higher conversions can also be achieved by a higher amount of catalyst while product selectivity is only a function of the suitability of the catalyst.

Selectivity:

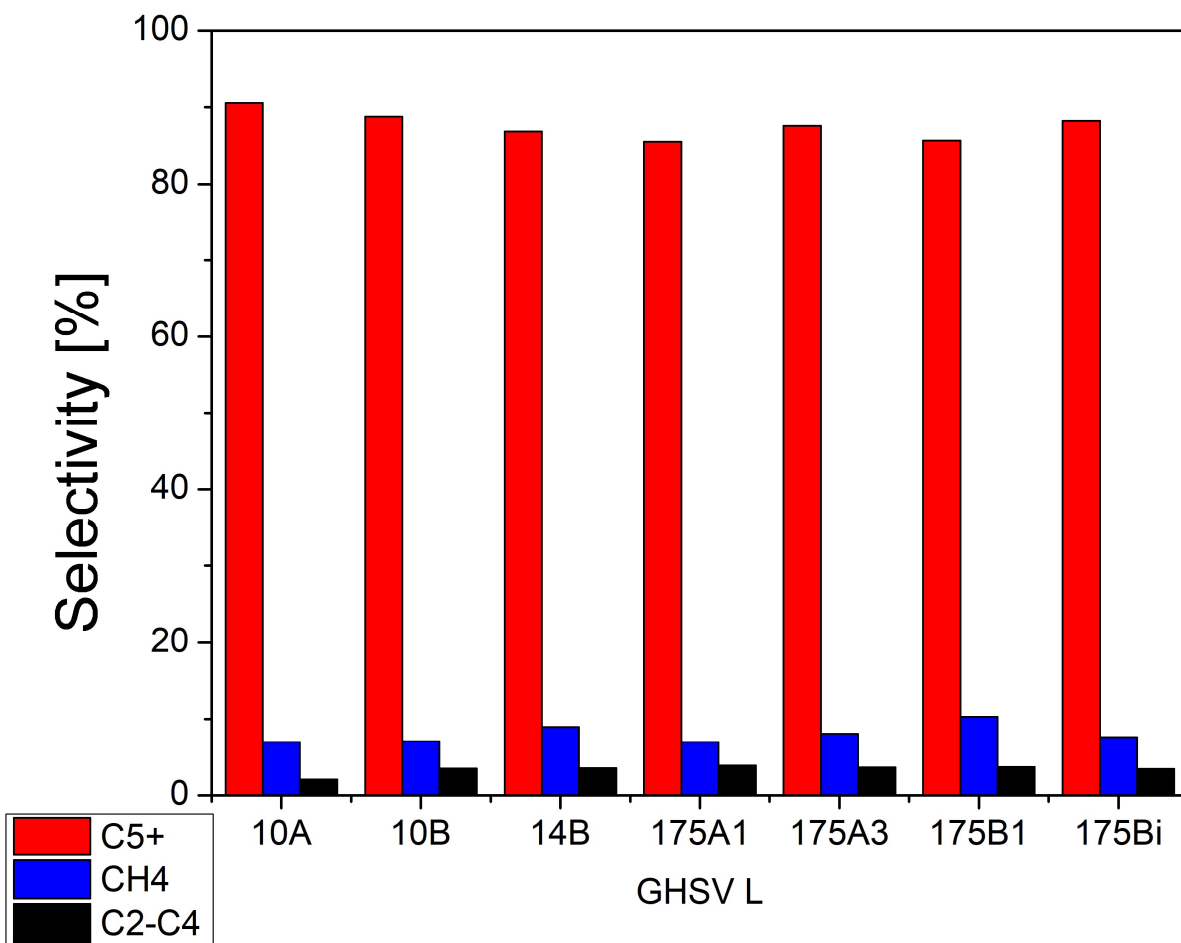


Figure 21: Selectivity at low GHSV.

Selectivity is analyzed at different GHSV. At low GHSV, Figure 21, the C₅₊ selectivity for all catalysts is over 85%, and the highest selectivity is achieved for the 10A catalyst, 10 wt% nominal Co loaded catalyst and calcined at 500°C. The selectivity to methane was below 10%, indicating that the Co catalysts are suited for the FTS, and the rest was distributed in the C₂-C₄ selectivity. For further discrimination between catalysts, the selectivity is analyzed at higher GHSVs.

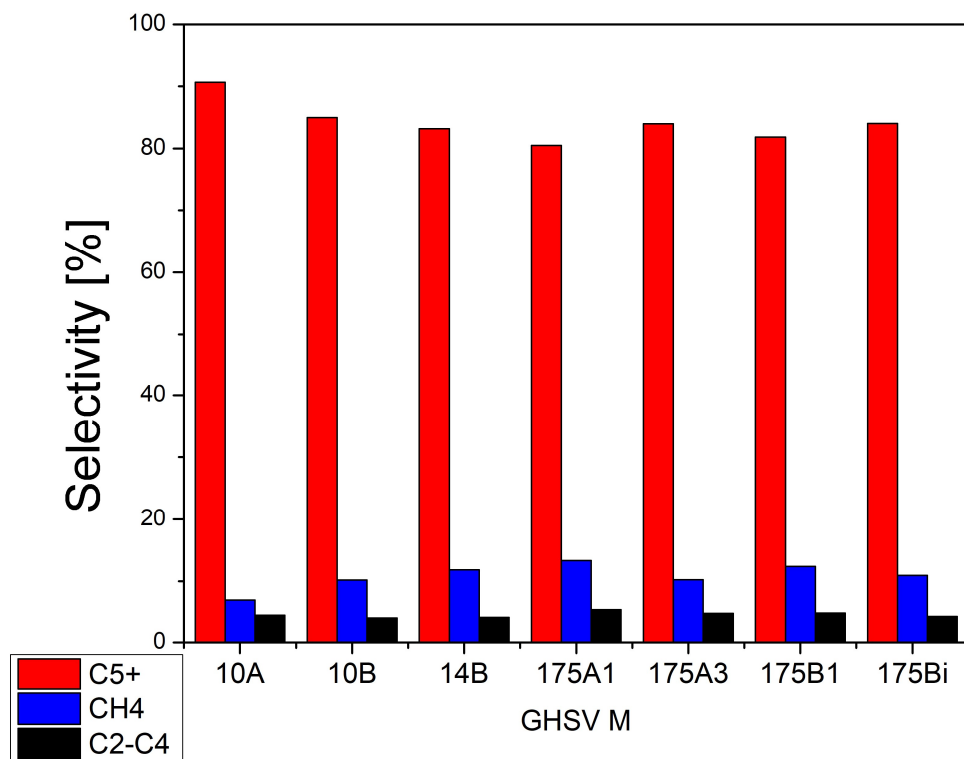


Figure 22: Selectivity at medium GHSV.

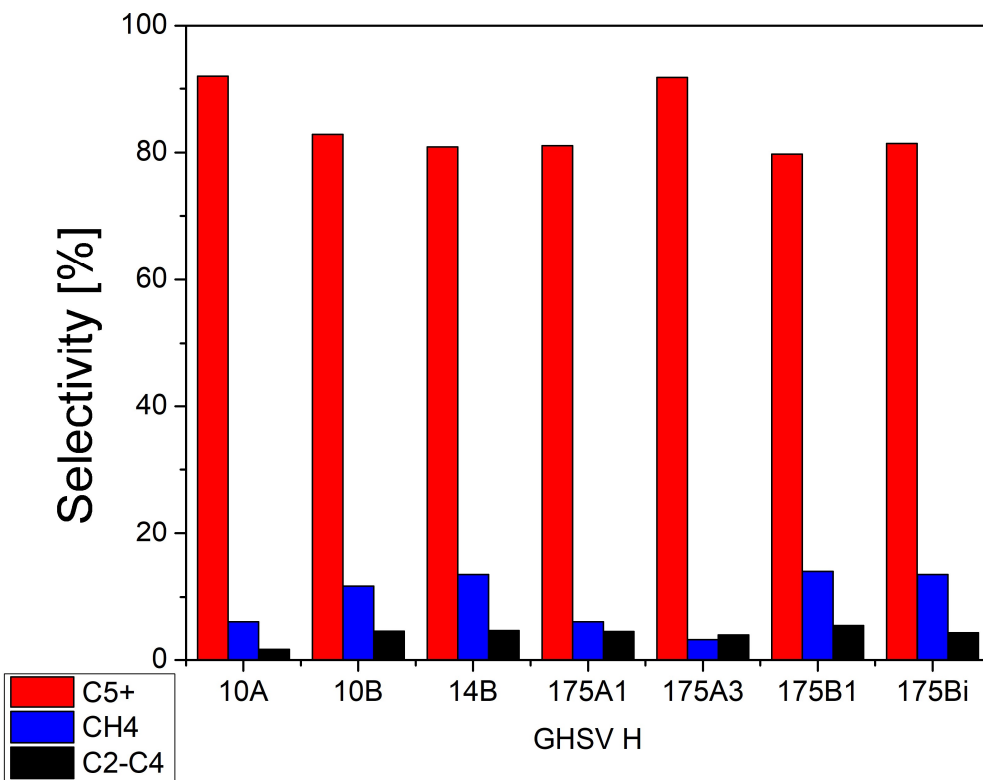


Figure 23: Selectivity at high GHSV.

The most C₅₊ selective catalyst at all GHSVs is the 10A, with a 10 wt% nominal cobalt loading and calcined at 500°C, as it can be seen in figures, 22,23. Nevertheless, catalyst 175A3, nominal cobalt loading of 17.5% calcined at 500°C and impregnated in 3 steps, emerges as one of the most C₅₊ selective catalysts. It is interesting to note that the catalysts calcined at 500°C show higher C₅₊ selectivity when working at high GHSV.

To choose the optimal catalyst, a catalyst with high selectivity is mandatory, but this cannot be done neglecting the conversion. So, to select the optimal catalyst, a balance between the selectivity and the conversion of the catalyst must be regarded, and that balance can be calculated by the productivity.

Productivity:

Productivity is a function of the conversion, selectivity and GHSV of the catalyst. Term “productivity” is assigned to the amount of liquids and waxes collected in the high-temperature (100 °C) trap. A catalyst with high selectivity and low conversion is not desirable, as neither a catalyst with high conversion and low C₅₊ conversion.

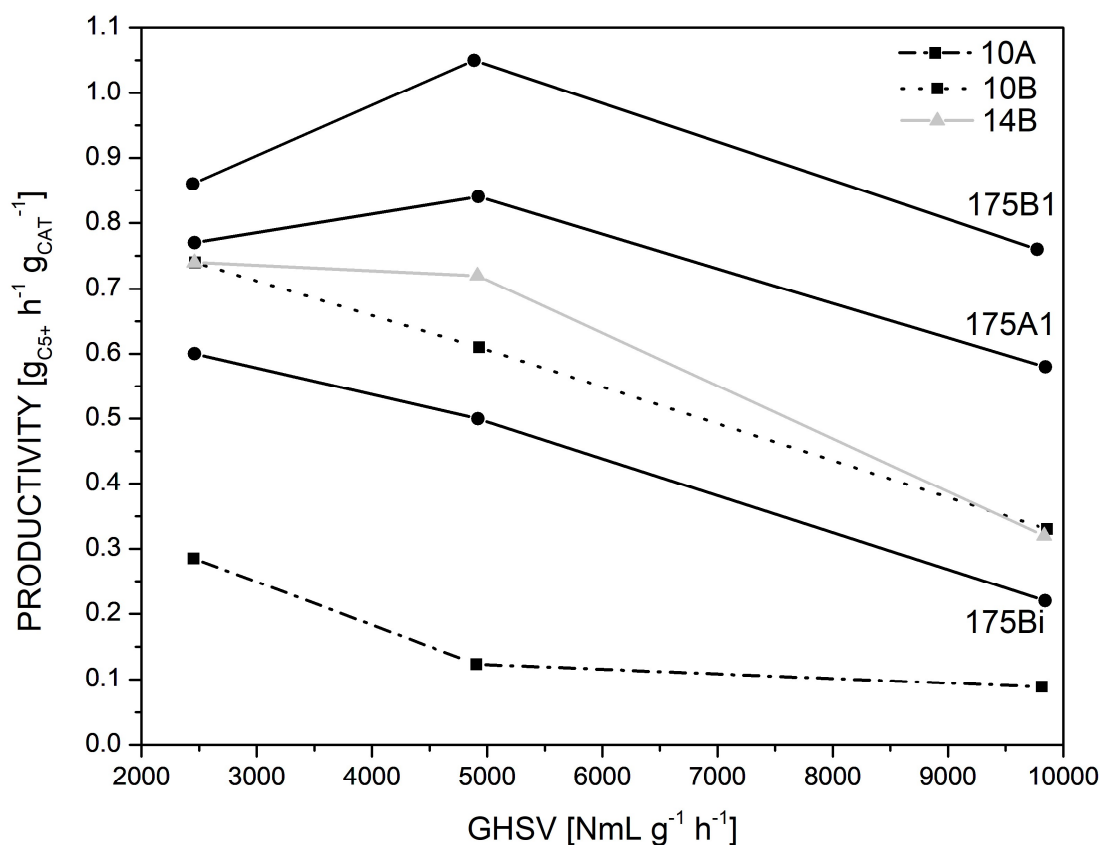


Figure 24: Productivity of liquids and waxes of the catalysts.

Productivity plays the role of relating these parameters together, allowing to select the optimal conditions of GHSV and catalyst, as it can be observed in Figure 24. With this figure it is easier to discriminate between the catalysts for selecting the optimal one.

For instance, the highest cobalt loading leads to higher productivity in comparison to the lower loadings, except for the catalyst 17.5Bi, with a 17.5 wt% Co loading, calcined at 275 °C between 3 impregnations. This behavior can be explained by the particle size and by the triple impregnation. When lower cobalt loading is impregnated, obtained particle sizes, of the cobalt oxides, tend to be smaller in comparison to the highest loading impregnation. The smallest particles tend to react with the support giving the inactive aluminate. This explanation is consistent with the 10 wt% loaded catalysts when analyzing the calcination temperatures.

Main Findings:

The Catalyst obtained by unique impregnation, calcinated at 275°C and loaded with 17.5wt% nominal Co content is selected as the optimal catalyst regarding the obtained productivity, as explained before in the main findings section, this can be explained by the lower loss of cobalt oxide by aluminate formation. The 17.5B1 catalyst has a selectivity over 80% for all the studied GHSVs and the best conversion in comparison with the other catalysts. without underestimating the fact that it yields the best productivity.

A lower calcination temperature for a fixed cobalt loading leads to better productivity of the catalysts, while a higher cobalt loading does not necessarily give a higher productivity, i.e., similar productivities of the 10B and 14B catalyst, and better performance in comparison with the 175Bi catalyst.

5.2.2. Ceria-promoted catalysts:

Once optimized the supported cobalt catalysts, choosing the 175B1 as the best catalyst of all the studied series. Ceria is promoted on a new batch of catalyst prepared following the same conditions as the 175B1. Ceria is promoted following the scheme, represented in Figure 25:

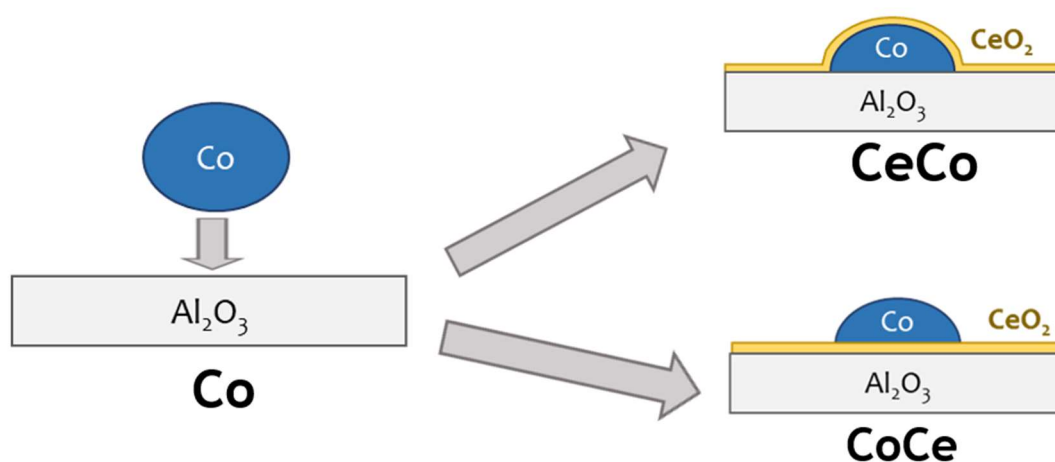


Figure 25: Scheme of the Ceria impregnation.

These new catalysts are put under catalytic testing with a syngas and a CO₂-Rich syngas (25 vol% CO₂) mixture at different temperatures for analyzing the effect of the Ceria at these different conditions. For the catalytic tests, an iso-conversion of 50% is aimed for all conditions. This is done for comparing purposes, as similar conversion is required for comparing the selectivity of the catalysts.

Conversion:

As for the prior section, the conversion of these catalysts is compared for obtaining an insight in the activity. Once obtained an insight in the activity of this catalytic material the selectivity of these materials is compared.

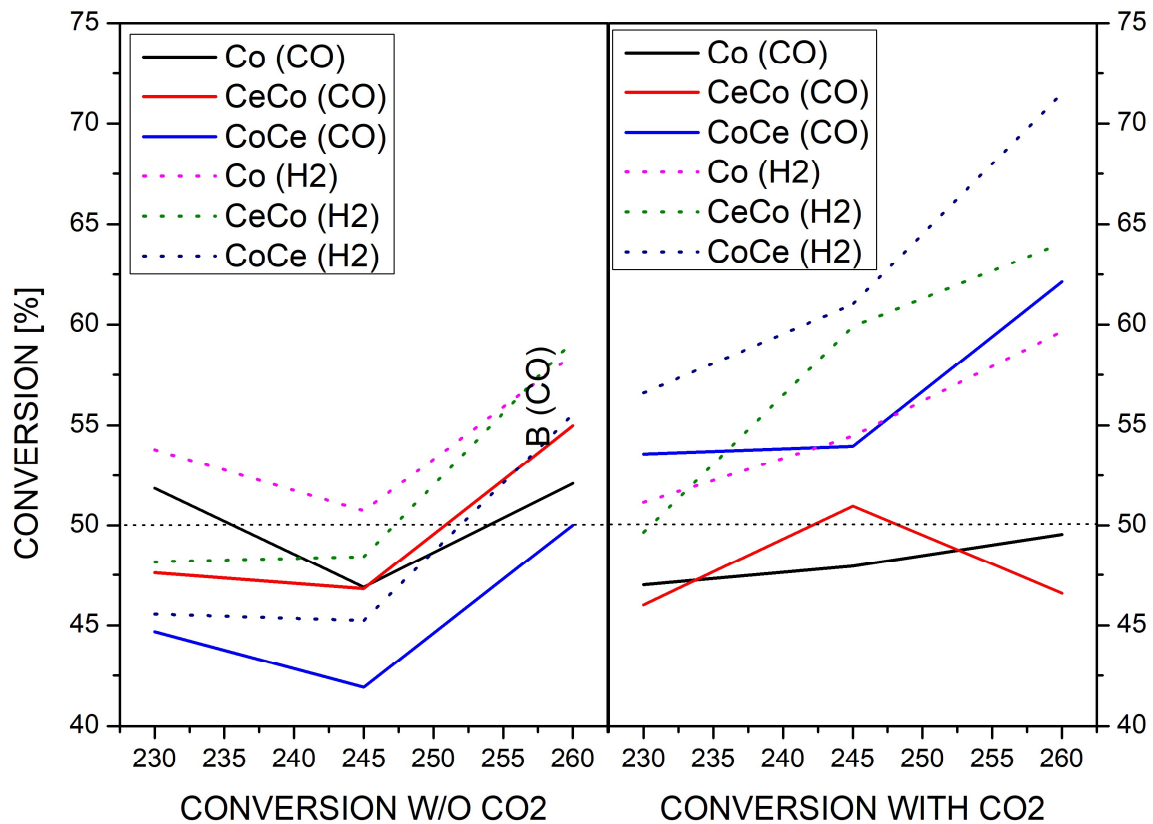


Figure 26: Conversion of the Ceria promoted catalysts at Syngas/CO₂-rich Syngas mixture.

In Figure 26, the dotted lines represent the conversion of the H₂. In the CO₂-free syngas, the conversion of the hydrogen and the monoxide are similar whilst at the CO₂-rich syngas mixture, a gap is found between the monoxide/H₂ conversion. This is due to the competence of the FTS and the reverse water gas shift reaction, in which both reactions compete in producing/consuming, respectively, the CO₂ present in the

mixture. Figure 26 is a graphical representation of the obtained conversions while trying to get the iso-conversion conditions.

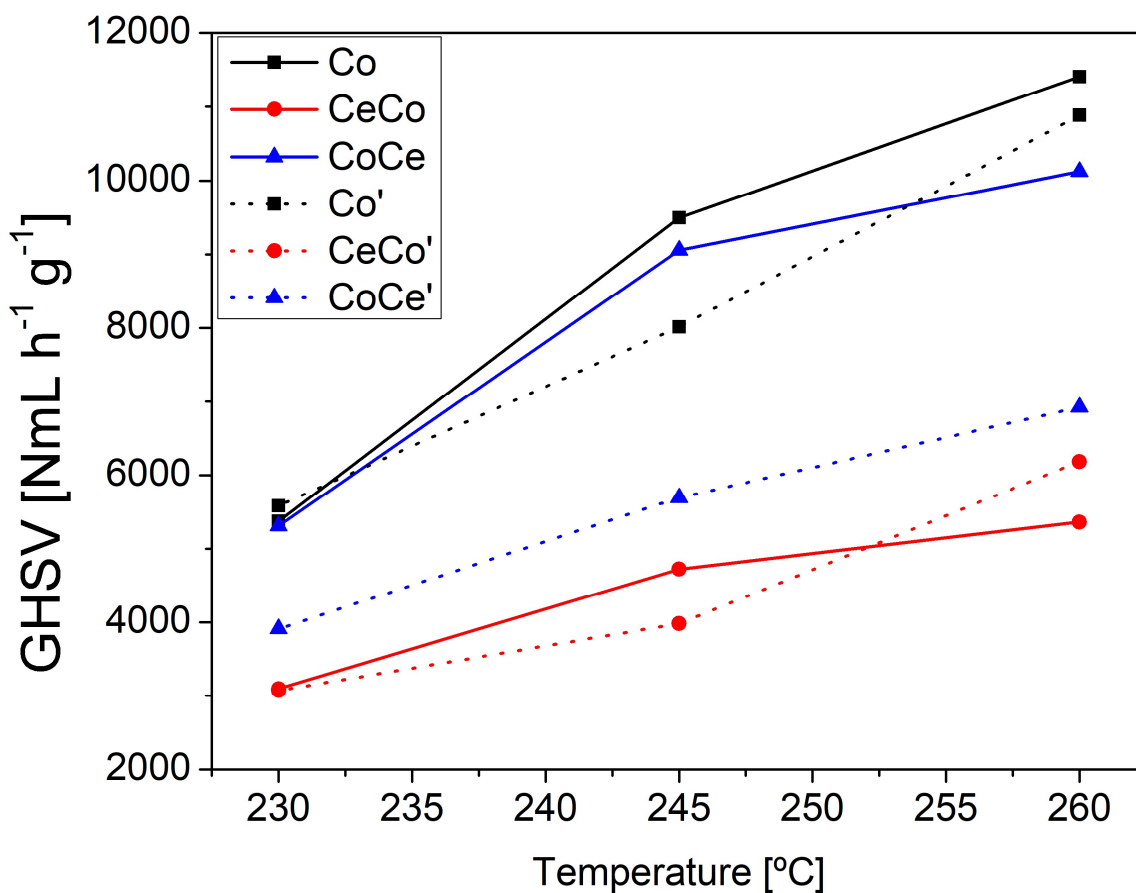


Figure 27: Estimated GHSVs for obtaining a 50% conversion.

The dotted lines in figure 27 represent the estimated GHSVs for the CO₂-rich syngas mixture. From the figure, the Co catalysts seem to be the most active ones while the CeCo catalysts are the least active, independent of the mixture used, while the CoCe catalyst behaves better for the CO₂-free syngas mixture.

Selectivity:

For these catalysts, the main objective was to maintain the conversion around 50%, in order to compare the selectivity. Selectivity is a function of the conversion, that is the reason why the iso-conversion is searched. For instance, we can have a very high conversion (>95%) with a high selectivity towards methane, which is a non-desirable scenario. Otherwise, having a high selectivity towards long-chain hydrocarbons with a low conversion is neither desirable.

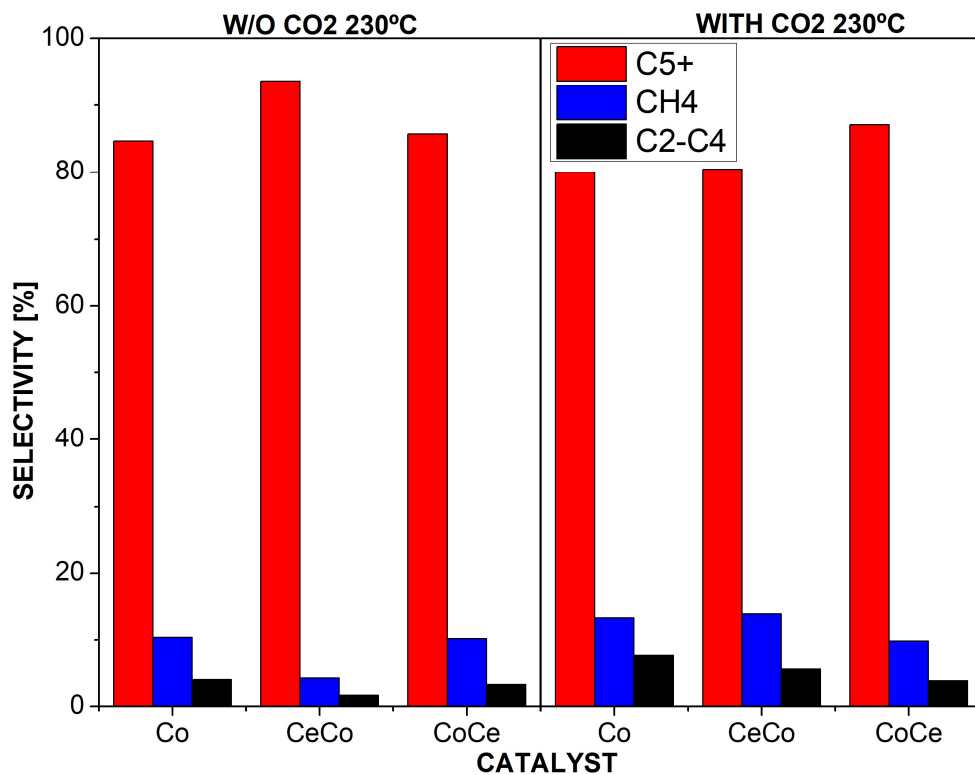


Figure 28: Selectivity of the Ceria-promoted catalysts at 230°C

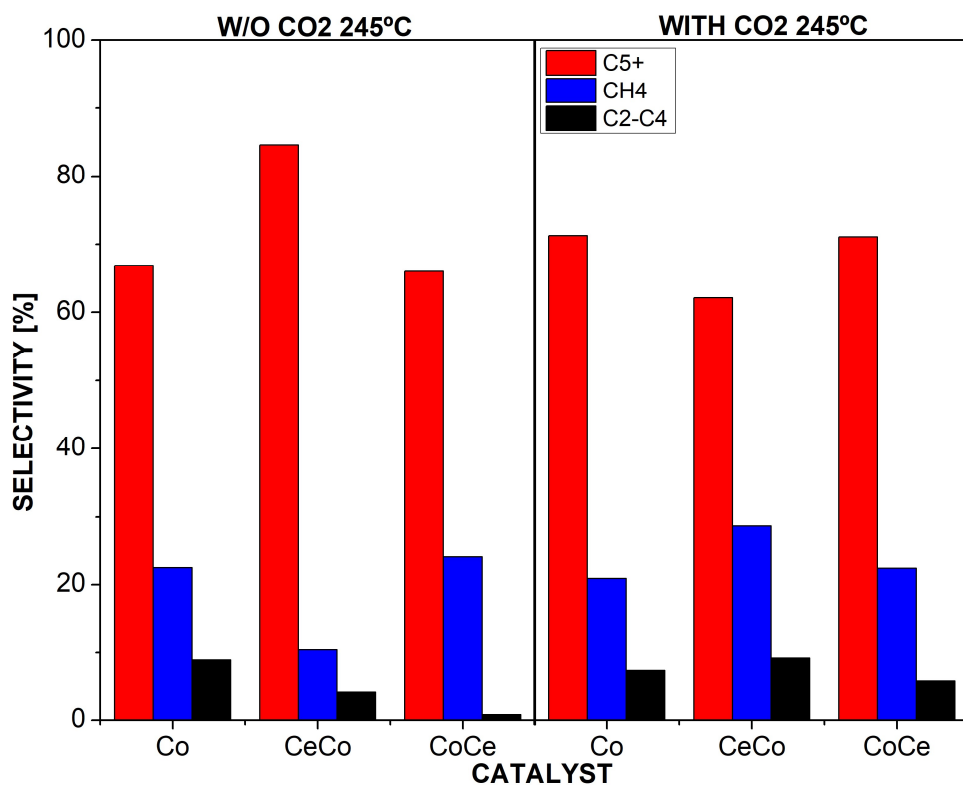


Figure 29: Selectivity of the Ceria-promoted catalysts at 245°C

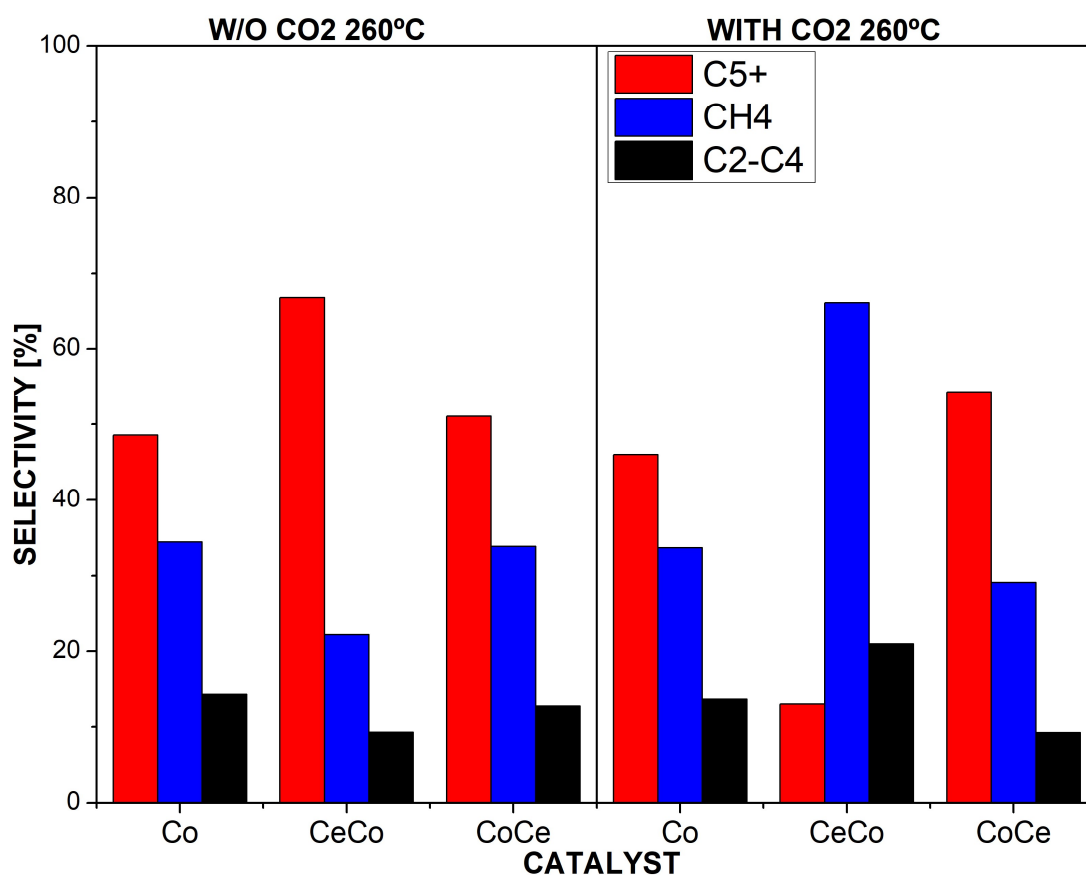


Figure 30: Selectivity of the Ceria-promoted catalysts at 260°C

In Figures 28-30, CeCo catalyst shows the highest C_{5+} selectivity reacting without CO_2 in the gas mixture. Notice that at lower temperature (Figure 29), the selectivity is above 90%; in Figure 30, the selectivity for the CeCo catalyst decreases to 85% approximately; and then at 260°C (Figure 31) the selectivity is located at 65%. This tendency can be observed for the rest of the catalysts, where C_{5+} selectivity is approximately 50% at the highest temperature conditions.

The scenario changes when the CO_2 -rich syngas mixture is used, for instance, in Figure 29, the CoCe catalyst has the highest C_{5+} selectivity, whilst in the CO_2 -free syngas mixture, the highest C_{5+} selectivity was obtained by the CeCo catalyst. A general behavior that can be seen for all temperatures, is that the highest C_{5+} selectivity for the CO_2 -free syngas is higher than the CO_2 -rich syngas.

For Figure 30, the C_{5+} selectivity is located at 85%, while at figure 30, C_{5+} selectivity of CoCe is equal to the one of the Co catalyst (~70%).

For figure 31, the behavior of the CeCo catalyst is radically different when the CO_2 -free or CO_2 -rich syngas mixture is used. For instance, when no CO_2 is present in the syngas, the CeCo catalyst has the best selectivity towards the C_{5+} fraction, while in the CO_2 -Rich syngas mixture the CeCo has the worst selectivity towards the C_{5+} fraction, by being highly selective to methane (over 65%), an undesired subproduct from

the FTS reaction, this result is congruent with the Ernst's observations (Ernst, Hilaire and Kiennemann 1999).

Another observation can be that the C_{5+} selectivity of CoCe is higher when CO_2 is present than when the CO_2 -free syngas is used for all temperatures. The Co catalyst has the same C_{5+} selectivity at 230°C and 260°C independently from the syngas mixture used, while at 245°C the selectivity when CO_2 is present the C_{5+} selectivity is slightly higher in comparison with the CO_2 -free conditions.

Ernst et al observes that formates on partially reduced ceria can be hydrogenated at temperatures higher than the formation of CH_4 , due to the hydrogenation of surface carbon obtained by dissociation of CO on metallic sites, thus explaining the higher selectivity in methane observed on Co±CeO₂/SiO₂ catalysts.

CO₂ Conversion:

CO₂ Conversion is a parameter for analyzing the effect of the CO₂ that is introduced in the system.

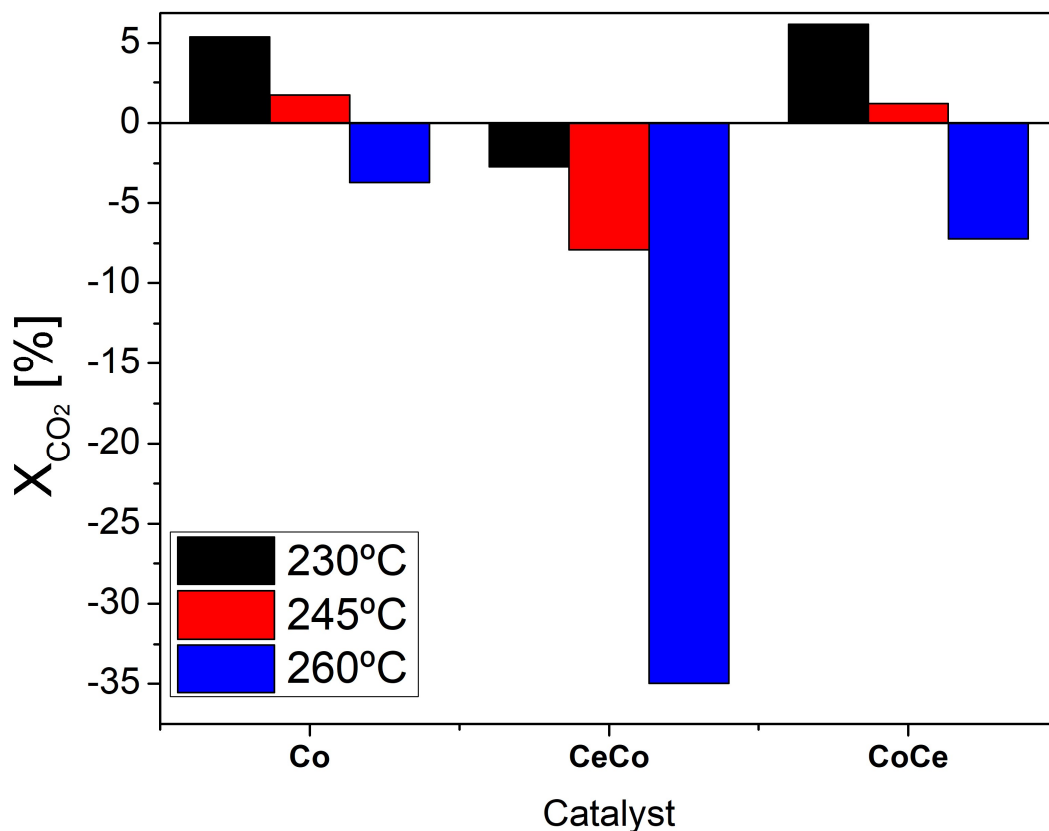


Figure 31: CO₂ conversion for the Ceria-promoted catalysts

In Figure 31, the CO₂ conversion of the catalysts is compared. At first glance, notable difference between catalysts can be detected. Negative conversion of CO₂ can be spotted, this negative conversion means that the CO₂ is produced in that catalytic test, whilst at a positive CO₂-conversion means a CO₂ transformation into products. The Cerium over Cobalt (CeCo) catalyst shows a strong tendency to produce CO₂, even at

low temperature, while the other catalysts tend to transform the CO₂ as a reactant at 230°C and 245°C, but all the catalysts show CO₂ production while working at 260°C.

An explanation of this behavior is that at lower temperatures, [T=230°C; 245°C], the decomposition and hydrogenation of the CO₂ is more suitable than its formation by the water gas shift reaction for the Co and CoCe catalysts, while for the CeCo catalyst the formation of the CO₂ is favored for all the temperatures. Citing Ernst's observations respecting the CeCo catalyst is that CO₂ production may be due to the CeOx network. This network can retain oxygen, so it could favor the formation of CO₂ through the reaction of the network-retained oxygen with the monoxide species captured by the surface species, whilst simultaneously favoring the formation of formates as seen earlier in the selectivity. Ernst et al, observes a higher methanation capacity of the Cerium promoted system. The enhanced formation of CO₂ and a higher methanation potential are coherent under the CeOx hypothesis and can explain the measured phenomena.

Productivity:

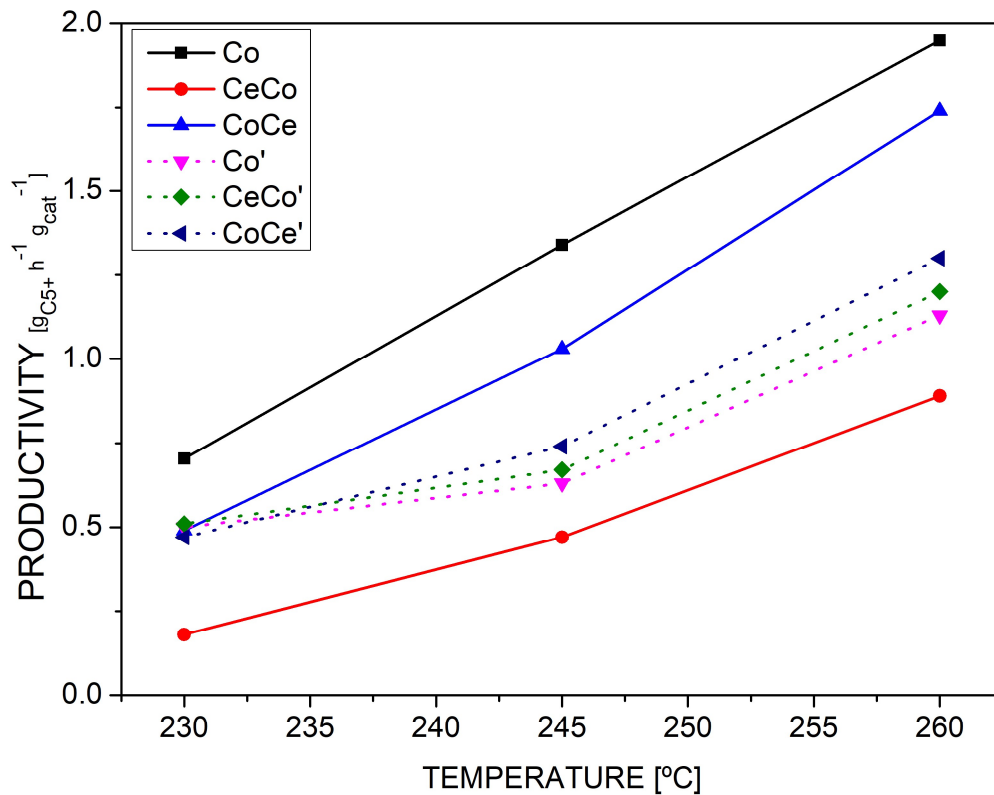


Figure 32: Productivity of the Catalysts. Dotted lines are selected for the CO₂-Rich syngas mixture.

From Figure 32, the least active catalyst is the CeCo in the pure syngas mixture, while for the same mixture, the most active catalyst is Co, by almost duplicating the productivity of CeCo at all temperatures.

When the role of the CO₂-rich syngas mixture is analyzed, a rapid conclusion can be drawn. The Productivity of these catalysts, especially at 260°C, is lower in comparison to the pure syngas mixture. This

result is expected because the CO₂ is not a reactive species in the FTS, and the role of the Ceria is to help transform this CO₂ with its chemophysical properties.

Nonetheless, even if productivity of the catalysts in presence of the CO₂ is below the productivity obtained for pure syngas, the catalysts promoted with Ce are more active than the Co one when CO₂ is present in the syngas mixture. The lowest productivity was obtained for the CeCo catalyst when tested under pure syngas mixture, while the Co catalyst performed worst, in terms of productivity, than the rest of catalysts when CO₂-rich syngas was used.

Discussion:

Lower production of C₅₊ hydrocarbons is obtained when CO₂ is present, the replacement of part of syngas by CO₂ led to lower catalytic activity, in comparison with the CO₂ free syngas. (Guilera, et al. 2022) correlates this effect to the lower partial pressure of the reactants, nonetheless, the results indicate a CO₂ transformation and conversion into other products is possible for 230°C and 245°C for the CoCe and Co Catalysts, while at 260°C all catalysts produced CO₂.

The Co catalyst emerges as the best catalyst, under the developed experiments, when working with pure syngas while the CoCe catalyst has the best performance when working with CO₂-rich syngas mixture.

The productivity for all catalysts increased with increasing temperature, this may seem counterintuitive because at higher temperatures a lower selectivity is achieved yet a higher GHSV is needed for maintaining the conversion in between the range of Conversion=[40-60%]. Thus, even with lower selectivity, a higher quantity of carbons is being transformed to C₅₊.

In conclusion, the transformation and conversion of CO₂ into products in the CO₂-rich syngas system is possible as shown in the results. Note that CO₂ was feed to the system at a 25 vol% and was successfully converted at 230 °C into other products. An interesting outlook could be an analysis to determine where do the CO₂ molecules go.

6. Conclusions:

The FTS catalytic performance of the reference micro-catalysts (Co/ γ -Al₂O₃) confirmed that the preparation and feed composition affected the conversion and the selectivity of the reaction. The calcination of the catalysts at higher temperature led to lost metallic surface area, to a lower dispersion of the catalyst, and to harder to reduce oxides. The highest Co loading gave the most productive catalyst, while a productivity comparison between the lowest and intermediate loaded catalysts didn't show significant difference. Unique impregnation gave the best properties of the catalysts in comparison to the triple impregnation.

The promotion with the Cerium oxide affected the properties of the catalysts, and showed particular behavior when CO₂ was present in comparison to the CO₂ free syngas. For instance, when working with syngas, the C₅₊ selectivity was enhanced for the Ce over Co (CeCo) catalyst in comparison to the other catalysts, whilst when CO₂ was present, this catalyst had the lowest C₅₊ selectivity. Interestingly, when working at the highest temperature, this catalyst predominantly produced methane, while in the CO₂-free syngas this catalyst had always the highest C₅₊ selectivity at all temperatures. The cerium oxide promotion had effect over the Co catalysts, and most importantly, its promotion on the catalyst. The order of impregnation of the cerium and cobalt showed to affect the catalytic behavior, as described in terms of selectivity.

The replacement of part of syngas by CO₂ led to lower catalytic activity, in comparison with the CO₂ free syngas. However, while nitrogen acts as an inert and standard, the CO₂ plays role as reactant on the conversion and selectivity of the FTS. In terms of productivity, the most productive catalysts are the Co one, when working with pure syngas. For the CO₂-rich syngas, CoCe catalyst gave the best productivity. The CoCe catalyst yields approximately 0.2 [g_{C₅₊}/h·g_{CAT}] less than the Co catalyst at all temperatures when no CO₂ is present in the syngas mixture whereas the difference in productivity tends to widen at higher temperatures when comparing the best catalysts of both systems.

Cerium impregnation is effective when CO₂ enriched syngas is used, the ceria promotion showed positive effect on the conversion of the CO₂ when impregnated before the Co, nonetheless, when working with pure syngas mixtures Co catalysts are recommended due to their higher productivity.

7. Outlook:

The results indicate that the experiments have achieved the proposed objectives. In order to improve with the results obtained and to gain further insight into the subject, it is recommended to study the impact of the following modifications:

- a) Increase in cobalt loading: it is observed that by increasing the cobalt loading from 10% by weight to 17.5%, productivity increases; this could suggest that working at higher cobalt loadings, e.g. wt%=[20%;25%], productivity would continue to increase.
- b) Decreased Ceria loading: Ceria promoted catalysts have obtained better productivity than unpromoted catalysts. The amount of ceria used was 10% and it is wanted to analyze if using a lower amount of ceria, for example wt% Ce=[0.5%; 1%;2%], would achieve the same performance.
- c) Increase of the CO₂ concentration: In the experiments in which a mixture rich in CO₂ was used, CO₂ was converted. The role of using an even more CO₂-rich mixture wants to be analyzed, for example, using a syngas mixture containing 50% CO₂, instead of the 25% CO₂ of the current mixture. It is believed that this could shift the FTS equilibrium and cause CO₂ transformation in the reaction.
- d) Carbon isotopes: Part of the CO₂ that is added as a reactant is consumed in the FTS, however, it is not known where it ends up and in what proportion it is transformed. Nevertheless, with isotope labeling, the CO₂ transformations can be traced. For example, Ernst et al, 1999, indicated that ceria systems tend to be very effective in hydrogenating formates, so it is very likely that much of this CO₂ ends up as methane.
- e) Hydrogen/Carbon Ratio: The syngas mixture containing CO₂ was hydrogen-depleted. This is because the ratio of hydrogen to total carbon was very low. It is congruent to think that the reaction was not completely favored, however working at a higher hydrogen concentration could facilitate the hydrogenation of the compounds and shift the equilibrium towards the products.

8. Bibliography

- Aligolzadeh, Hamed, Ali Jebreili Jolodar, Rasool Mohammadikhah, and Duc Pham. 2015. "CFD analysis of hot spot formation through a fixed bed reactor of Fischer-Tropsch synthesis." *Cogent Engineering* 1006016. doi:10.1080/23311916.2015.1006016.
- Arsalanfar, M., A. A. Mirzaei, H. R. Bozorgzadeh, H. Atashi, S. Shahriari, and A. Pourdolat. 2012. "Structural characteristics of supported cobalt–cerium oxide catalysts used in Fischer–Tropsch synthesis." *Journal of Natural Gas Science and Engineering* 119-129. doi:10.1016/j.jngse.2012.05.015.
- Berger, Rob J., Javier Pérez-Ramírez, Freek Kapteijn, and Jacob A. Moulijn. 2002. "Catalyst performance testing: bed dilution revisited." *Chemical Engineering Science* 4921-4932. doi:10.1016/S0009-2509(02)00273-7.
- Bezemer, G. Leendert, Johannes H. Bitter, Herman P. C. E. Kuipers, Heiko Oosterbeek, Johannes E. Holewijn, Xiaoding Xu, Freek Kapteijn, A. Jos van Dillen, and Krijn P. de Jong. 2006. "Cobalt particle size effects in the Fischer-Tropsch reaction studied with carbon nanofiber supported catalysts." *J Am Chem Soc* 3956-3964. doi:10.1021/ja058282w.
- Borg, Øyvind, Sigrid Eri, Edd A. Blekkan, Sølvi Storsæter, Hanne Wigum, Erling Rytter, and Anders Holmen. 2007. "Fischer–Tropsch synthesis over γ -alumina-supported cobalt catalysts: Effect of support variables." *Journal of Catalysis* 89-100. doi:10.1016/j.jcat.2007.03.008.
- Clarkson, J., P. R. Ellis, R. Humble, G. J. Kelly, M. McKenna, and J. West. 2018. "Deactivation of alumina supported cobalt FT catalysts during testing in a Continuous-stirred tank reactor (CSTR)." *Applied Catalysis A: General* 28-37.
- Davis, Burtron H. 2005. "Fischer-Tropsch synthesis: Overview of reactor development and future potentialities." *Catalysis* 3-4. doi:10.1007/s11244-005-2886-5.
- Ernst, B, L Hilaire, and A Kiennemann. 1999. "Effects of highly dispersed ceria addition on reducibility, activity and hydrocarbon chain growth of a Co/SiO₂ Fischer–Tropsch catalyst." *Catalysis Today* 413-427. doi:10.1016/S0920-5861(98)00519-7.
- Fratolocchi, Laura, Gianpiero Groppi, Carlo Giorgio Visconti, Luca Lietti, and Enrico Tronconi. 2020. "On the passivation of platinum promoted cobalt-based Fischer-Tropsch catalyst." *Catalysis Today* 79-87. doi:10.1016/j.cattod.2019.02.069.
- Gregg, S.J., and K.S.W. Sing. 1982. *Adsorption, Surface Area and Porosity*. London: Academic Press.
- Guilera, Jordi, José Antonio Díaz-López, Antonio Berenguer, Martí Biset-Peiró, and Teresa Andreu. 2022. "Fischer-Tropsch synthesis: Towards a highly-selective catalyst by lanthanide promotion under relevant CO₂ syngas mixtures." *Applied Catalysis A: General* 118423.
- Hickman, Daniel A, John C Degenstein, and Fabio H Ribeiro. 2016. "Fundamental principles of laboratory fixed bed reactor design." *Current Opinion in Chemical Engineering* 1-9. doi:10.1016/j.coche.2016.07.002.

- Iglesia, Enrique. 1997. "Design, synthesis, and use of cobalt-based Fischer-Tropsch synthesis catalysts." *Applied Catalysis A: General* 59-78. doi:[https://doi.org/10.1016/S0926-860X\(97\)00186-5](https://doi.org/10.1016/S0926-860X(97)00186-5).
- Jones, Mitchell P., Theresa Krexner, and Alexander Bismarck. 2022. "Repurposing Fischer-Tropsch and natural gas as bridging technologies for the energy revolution." *Energy: Conversion and Management* 115882. doi:doi.org/10.1016/j.enconman.2022.115882.
- Kraum, Martin, and Manfred Baerns. 1999. "Fischer–Tropsch synthesis: the influence of various cobalt compounds applied in the preparation of supported cobalt catalysts on their performance." *Applied Catalysis A: General* 189-200. doi:[10.1016/S0926-860X\(99\)00172-6](https://doi.org/10.1016/S0926-860X(99)00172-6).
- Mahmoudi, Hamid, Mahmoudi Maedeh, Doustdar Omid, Jahangiri Hessam, Tsolakis Athanasios, Gu Sai, Miroslaw, and Lech Wyszynski. 2017. "A review of Fischer Tropsch Synthesis process, mechanism, surface chemistry and catalyst formulation." *Biofuels Eng.* 11-31. doi:doi.org/10.1515/bfuel-2017-0002.
- Małecka, Barbara, Łącz Agnieszka, Drożdż Ewa, and Małecko Andrzej. 2015. "Thermal decomposition of d-metal nitrates supported on alumina." *Journal of Thermal Analysis and Calorimetry* 1053-1061.
- Martinelli, Michela, Muthu Kumaran Gnanamani, Steve LeViness, Gary Jacobs, and Wilson D. Shafer. 2020. "An overview of Fischer-Tropsch Synthesis: XTL processes, catalysts and reactors." *Applied Catalysis A: General* 117740. doi:[10.1016/j.apcata.2020.117740](https://doi.org/10.1016/j.apcata.2020.117740).
- Micromeritics. n.d. *BJH Pore Volume and Area Distributions*. Accessed 6 13, 2023. <https://notebook.community/RJC0514/micromeritics/documentation/BJH>.
- Mirzaei, A. A., M. Galavy, A. Beigbabaei, and V. Eslamimanesh. 2007. "Preparation and operating conditions for cobalt cerium oxide catalysts used in the conversion of synthesis gas into light olefins." *JICS* 347-363.
- Mirzaei, Ali, Maryam Arsalanfar, Hamid Bozorgzadeh, and Abdoreza Samimi. 2014. "A review of Fischer-Tropsch synthesis on the cobalt based catalysts." *Physical Chemistry Research*. doi:[10.22036/pcr.2014.5786](https://doi.org/10.22036/pcr.2014.5786).
- Nissinen, Terhi, Markku Leskelä, Michael Gasik, and Jaakko Lamminen. 2005. "Decomposition of mixed Mn and Co nitrates supported on carbon." *Thermochimica Acta* 155-161. doi:[10.1016/j.tca.2004.09.005](https://doi.org/10.1016/j.tca.2004.09.005).
- OHSU, Oregon Health & Science University. 2023. *ICP-MS as a Technique*. Accessed April 20, 2023. <https://www.ohsu.edu/elemental-analysis-core/icp-ms-technique>.
- Pardo-Tarifa, Fatima, Saúl Cabrera, Margarita Sanchez-Dominguez, and Magali Boutonnet. 2017. "Ce-promoted Co/Al₂O₃ catalysts for Fischer–Tropsch synthesis." *International Journal of Hydrogen Energy* 9754-9765. doi:[10.1016/j.ijhydene.2017.01.056](https://doi.org/10.1016/j.ijhydene.2017.01.056).
- Rouquerol, Françoise, Jean Rouquerol, and Kenneth Sing. 1999. "CHAPTER 7 - Assessment of Mesoporosity." In *Adsorption by Powders and Porous Solids*, by Françoise Rouquerol, Jean Rouquerol and Kenneth Sing, 191-217. London: Academic Press.

- Shehesh, Shivananda Ali, and S. Dasappa. 2016. "Biomass to liquid transportation fuel via Fischer-Tropsch synthesis- Technology review and current scenario." *Renewable and sustainable energy reviews* 267-286. doi:dx.doi.org/10.1016/j.rser.2015.12.143.
- Thommes, M. 2010. "Physical Adsorption Characterization of Nanoporous Materials." *Chemie Ingenieur Technik* 1059-1073. doi:10.1002/cite.201000064.
- Thommes, Matthias, Katsumi Kaneko, Alexander V. Neimark, James P. Olivier, Francisco Rodriguez-Reinoso, Jean Rouquerol, and Kenneth S. W. Sing. 2015. "Physisorption of gases, with special reference to the evaluation of surface area and pore size distribution (IUPAC Technical Report)." *Pure and Applied Chemistry* 1051-1069. doi:10.1515/pac-2014-1117.
- UN, General Assembly. 2015. *Transforming our world: the 2030 Agenda for Sustainable*. Resolution, General Assembly of the UN. <https://documents-dds-ny.un.org/doc/UNDOC/GEN/N15/291/89/PDF/N1529189.pdf?OpenElement>.
- van de Loosdrecht, J., M. van der Haar, A. M. van der Kraan, A. J. van Dillen, and J. W. Geus. 1997. "Preparation and properties of supported cobalt catalysts for Fischer-Tropsch synthesis." *Applied Catalysis A: General* 365-376. doi:10.1016/S0926-860X(96)00306-7.
- VAN NUFFEL, Luc, João GORENSTEIN DEDECCA, Tycho SMIT, and Koen RADEMAEKERS. 2018. *Sector coupling: how can it be enhanced in the EU to foster grid stability and decarbonise?* Study, Brussels: European Parliament.
- Zeng, Shanghong, Yong Du, Haiquan Su, and Yulong Zhang. 2011. "Promotion effect of single or mixed rare earths on cobalt-based catalysts for Fischer-Tropsch synthesis." *Catalysis Communications* 6-9.
- Zhang, Lingling, Lihui Dong, Wujiang Liu, Lianjun Yu, Yu Deng, Bin Liu, Haiqin Wan, C Gao, Keqin Sun, and Lin Dong. 2011. "Effect of cobalt precursors on the dispersion, reduction, and CO oxidation of CoO / γ -Al₂O₃ catalysts calcined in N₂." *Journal of Colloid and Interface Science* 464-471. doi:10.1016/j.jcis.2010.11.076.